Analysis of subthreshold antiproton production in p-nucleus and nucleus-nucleus collisions in the relativistic Boltzmann-Uehling-Uhlenbeck approach

Stefan Teis, Wolfgang Cassing, Tomoyuki Maruyama,* and Ulrich Mosel
Institut für Theoretische Physik, Universität Giessen, D-35392 Giessen, Germany
(Received 13 January 1994)

We calculate the subthreshold production of antiprotons in the Lorentz-covariant relativistic Boltzmann-Uehling-Uhlenbeck (RBUU) approach employing a weighted test particle method to treat the antiproton propagation and absorption nonperturbatively. We find that the antiproton differential cross sections are highly sensitive to the baryon and antiproton self-energies in the dense baryonic environment. Adopting the baryon scalar and vector self-energies from the empirical optical potential for proton-nucleus elastic scattering and from Dirac-Brueckner calculations at higher density $\rho > \rho_0$ we examine the differential antiproton spectra as a function of the antiproton self-energy. A detailed comparison with the available experimental data for p-nucleus and nucleus-nucleus reactions shows that the antiproton feels a moderately attractive mean field at normal nuclear matter density ρ_0 which is in line with a dispersive potential extracted from the free annihilation cross section.

PACS number(s): 25.75.+r, 24.10.Jv, 24.10.Cn, 21.65.+f

I. INTRODUCTION

The production of particles at energies below the free nucleon-nucleon threshold (subthreshold production) constitutes one of the most promising sources of information about the properties of nuclear matter at high densities since the particles are produced predominantly during the compressed stage at high density [1–4]. Antiproton production at energies of a few GeV/nucleon is the most extreme subthreshold production process and has been observed in proton-nucleus collisions already more than 20 years ago [5–7]. Experiments at the JINR [8] and at the BEVALAC [9,10] have provided, furthermore, the first measurements of subthreshold antiproton production in nucleus-nucleus collisions. Since then the problem was taken up again at KEK [11] and GSI [12] with new detector setups. Various descriptions for these data have been proposed. Based on thermal models it has been suggested that the antiproton yield contains large contributions from $\Delta N \rightarrow \bar{p} + X$, $\Delta\Delta \rightarrow \bar{p} + X$, and $\rho\rho \rightarrow \bar{p}N$ production mechanisms [13–15]. Other models have attempted to explain these data in terms of multiparticle interactions [16].

In a first chance nucleon-nucleon collision model (assuming high-momentum tails consistent with data on backward proton scattering) Shor *et al.* [17] succeeded in reproducing the antiproton yield for the proton-nucleus case; however, these authors underestimated the yield by more than 3 orders of magnitude for nucleus-nucleus collisions. This problem was partly resolved by Batko *et al.* [18] who performed the first nonequilibrium $\bar{p}$-production study on the basis of the VUU transport equation. Essential for this success was that in $A + A$ reactions the dominant production channel proceeds via an intermediate nucleon resonance which allows storing a sizeable amount of energy that can be used in a subsequent collision for the production of a $p\bar{p}$ pair. Later on, these findings were also confirmed by Huang *et al.* [19].

These results have led to the suggestion that the quasiparticle properties of the nucleons might be important for the $\bar{p}$ production process which becomes more significant with increasing nuclear density. Schaffner *et al.* [20] found in a static thermal relativistic model, assuming kinetic and chemical equilibrium, that the $\bar{p}$ abundance might be dramatically enhanced when assuming the antiproton self-energy to be given by charge conjugation of the nucleon self-energy. This leads to strong attractive vector self-energies for the antiprotons. However, the above concept lacks unitarity between real and imaginary part of the $\bar{p}$ self-energy and thus remains questionable. Besides this, even in the σ-ω model the Fock terms lead to a suppression of the attractive $\bar{p}$ field [21], such that the production threshold is shifted up in energy again as compared to the simple model involving charge conjugation. Furthermore, the assumption of thermal and especially chemical equilibrium most likely is not fulfilled, e.g., in Si+Si collisions around 2 GeV/nucleon [22].

Preliminary results of a fully relativistic transport calculation for antiproton production including $\bar{p}$ annihilation as well as the change of the quasiparticle properties in the medium have been reported in [23]. There it was found that according to the reduced nucleon mass in the medium the threshold for $\bar{p}$ production is shifted to lower energy and the antiproton cross section prior to annihilation becomes enhanced for Si+Si at 2.1 GeV/nucleon by approximately a factor 70 as compared to a relativistic cascade calculation where no in-medium effects

*Permanent address: Department of Physics, Kyoto-University, Kyoto, Japan.

are incorporated. However, all these transport calculations [18,19,23] suffered from an approximate geometrical treatment of the very strong annihilation channel and a neglect of the momentum dependence of the baryon self-energies.

In our present work we therefore analyze the production of antiprotons in the framework of the relativistic transport theory (RBUU) where antiprotons are propagated explicitly in the respective time-dependent potentials and their annihilation is calculated nonperturbatively by means of individual rate equations.

First results have been published in [24]. Results of a very similar investigation by Li *et al.* [25] have recently become available and we compare frequently with the outcome of this study.

In this respect we first discuss two simple models for the $\bar{p}$ self-energy in Sec. II and present the general transport equations for nucleons and antinucleons in Sec. III. The numerical implementation of $\bar{p}$ production is presented in Sec. IV as well as a detailed analysis of the production process with respect to the self-energies employed, the systematic with respect to projectile and target masses, and the individual baryonic production channels. In Sec. V we present the treatment of $\bar{p}$ propagation and annihilation and discuss the geometrical aspects of $\bar{p}$ absorption. The explicit comparison of our calculations with the available experimental data for $p+A$ and $A+A$ reactions is performed in Sec. VI, while a summary on the $\bar{p}$ self-energies concludes the paper in Sec. VII.

II. MODELS FOR THE ANTIPROTON SELF-ENERGY

The dynamics and the properties of particles in a many-body system strongly depend on their mutual interactions with the surrounding particles and are reflected in their self-energies. While the real part of the self-energy describes the change of the particle momenta in the medium, all inelastic reaction channels as well as elastic-scattering processes are accounted for by the imaginary part of the self-energy $\Sigma(p_\mu, \rho_s, j_\mu)$. If the self-energy Σ is an analytic function of the particle energy $\epsilon = p_0$, its imaginary and real part are related up to a constant by the dispersion relations:

$$\mathrm{Re}\,[\Sigma(\epsilon)] = \frac{1}{\pi} P \int_0^{+\infty} \frac{\mathrm{Im}\,[\Sigma(\epsilon')]}{\epsilon' - \epsilon} d\epsilon', \tag{1}$$

$$\mathrm{Im}\,[\Sigma(\epsilon)] = -\frac{1}{\pi} P \int_0^{+\infty} \frac{\mathrm{Re}\,[\Sigma(\epsilon')]}{\epsilon' - \epsilon} d\epsilon'. \tag{2}$$

Since we assume particles and antiparticles to be different particle species, the integration in the principal-value integrals (1) and (2) extends only over positive energies.

In the relevant energy regime (1–5 GeV/nucleon) of heavy-ion collisions and proton-nucleus collisions the self-energies of baryons and antiprotons are known to be quite different. The $\bar{p}$ self-energy is dominated by the antiproton annihilation with baryons ($\bar{p} + B \to X$) as shown by low-energy antiproton-nucleon scattering experiments at LEAR [26,27]. Since the antiproton production probability at subthreshold energies is extremely low, the number of antiprotons produced in heavy-ion collisions and proton-nucleus collisions is negligible compared to the number of baryons involved in the reaction. Thus contributions from elastic $\bar{p}$-$\bar{p}$ scattering to the antiproton self-energy can be neglected as well as contributions of $\bar{p}$-annihilation channels to the baryon self-energies.

A. A dispersive model

In the following we present a simple model for the real part of the $\bar{p}$ self-energy using the dispersion relation (1). In the low-density limit the imaginary part of the self-energy (neglecting elastic scattering) is given by the integral:

$$2\,\mathrm{Im}\,\Sigma_{\bar{p}}(x, \Pi_{\bar{p}}) = -\frac{4}{(2\pi)^3} \int d^3\Pi_B \frac{m_B^*}{\Pi_B^0} \times W(\Pi_{\bar{p}}^\mu, \Pi_B^\mu) f(x, \Pi_B), \tag{3}$$

where $W(\Pi_{\bar{p}}^\mu, \Pi_B^\mu)$ is the probability of an antiproton with momentum $\Pi_{\bar{p}}^\mu$ to annihilate in a collision with a baryon of effective mass m^* and momentum Π_B^μ. $f(x, \Pi_B)$ is the baryon phase-space distribution function at space-time x, whereas the factor 4 in formula (3) arises from the summation over the spin and isospin degrees of freedom. We simplify this expression by considering an antiproton moving in infinite nuclear matter of density ρ_0 ($= 0.171/\mathrm{fm}^3$) at rest, i.e., $\mathbf{\Pi}_B = 0$. Both the antiprotons and the baryons now are supposed to have effective masses equal to the rest mass of the nucleon. This leads to the following analytic expression for the $\bar{p}$-annihilation probability

$$W(\Pi_{\bar{p}}^\mu, \Pi_B^\mu) = \frac{\sqrt{{\Pi_{\bar{p}}^0}^2 - m_N^2}}{\Pi_{\bar{p}}^0} \sigma_{\mathrm{abs}}(\Pi_{\bar{p}}^0), \tag{4}$$

where σ_{abs} is the total $\bar{p}$-annihilation cross section. Due to the above assumptions the integral over the baryon phase-space distribution function and the summation over the spin and isospin degrees of freedom in Eq. (3) can be replaced by a multiplication of the annihilation probability with ρ_0. The expression for the imaginary part of the antiproton self-energy as a function of the antiproton energy then reads

$$\mathrm{Im}\,\Sigma_{\bar{p}}(\Pi_{\bar{p}}^0) = -\frac{1}{2} \frac{\sqrt{{\Pi_{\bar{p}}^0}^2 - m_N^2}}{\Pi_{\bar{p}}^0} \cdot \sigma_{\mathrm{abs}}(\Pi_{\bar{p}}^0)\, \rho_0, \tag{5}$$

and the real part of Σ at density ρ_0 can be calculated from Eq. (3) by employing the dispersion relation (1). We expect this expression to give a reasonable description of $\mathrm{Im}\Sigma_{\bar{p}}$ at least for densities up to ρ_0 where possible medium corrections to σ_{abs} are still small.

In order to estimate $\mathrm{Re}\Sigma(\epsilon)$ at ρ_0 we adopt the parametrization from [13] for σ_{abs}, i.e.,

$$\sigma_{\mathrm{abs}} = \sigma_0 \frac{s_0}{s} \left(\frac{A^2\, s_0}{(s - s_0)^2 + A^2\, s_0} + B \right) \tag{6}$$

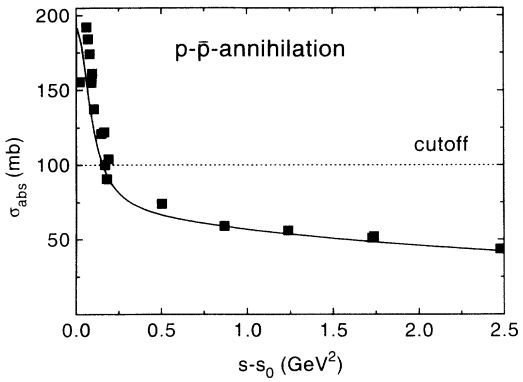

FIG. 1. Free annihilation cross section for $\bar{p}+p \to X$. Dots: experimental data from [28]; solid line: parametrization (6).

with the constants $\sigma_0 = 120$ mb, $A = 50$ MeV, $B = 0.6$, and $s_0 = 4m_N^2$. Figure 1 displays this parametrization in comparison to the experimental data for the free cross section taken from [28] as a function of $s - s_0$ where s is the invariant energy squared. The result of this calculation for $\mathrm{Re}\Sigma(\epsilon)$ is displayed in Fig. 2 as a function of the $\bar{p}$-kinetic energy. In order to investigate the sensitivity of this result to the parametrization of the absorption cross section, we used, in addition, different parameters B (cf. Fig. 2) to vary the overall size of σ_{abs}. For an antiproton at rest we find values for the real part of the self-energy of -175 MeV up to -100 MeV. While we observe a steep rise for small kinetic energies, this flattens out for higher energies and reaches an asymptotic value of 0 to -10 MeV. Furthermore, the variation in the cross section mainly affects the low-energy regime. The $\bar{p}$ self-energies obtained in the framework of this simple model are well in line with the potential analysis for $\bar{p} + A$ reactions by Janouin *et al.* [29].

B. Mean-field models

We now turn to the treatment of the antiproton self-energies in mean-field models where the imaginary part of the self-energies is not included at all, thus inherently violating the dispersion relations (1, 2).

As an example, we consider the mean-field approximation of the familiar $\sigma - \omega$ model [30] where only momentum-independent vector $U_v^\mu(x)$ and scalar parts $U_s(x)$ of the self-energies are taken into account. The equation of motion for a fermion spinor then reads

$$\left\{\gamma^\mu \left[i\partial_\mu - U_\mu^v(x)\right] - \left[m + U^s(x)\right]\right\} \Psi(x) = 0, \qquad (7)$$

while the equation of motion for antiparticles is obtained by applying the charge conjugation operator to this equation. As a consequence the scalar part of the self-energy is the same for particles and antiparticles, while the vector part of the antiparticle potential changes the sign

$$U_{C\,\mu}^v(x) = -U_\mu^v(x), \qquad (8)$$

$$U_C^s(x) = U^s(x). \qquad (9)$$

The combination of both parts of the antiparticle self-energy to the Schrödinger-equivalent potential in the non-relativistic limit leads to a strongly attractive potential for the antiprotons when using the original coupling constants from [30]. The value of the Schrödinger-equivalent potential at $\rho = \rho_0$ is approximately -700 MeV for $\epsilon = 0$ and becomes even more attractive with increasing kinetic energy of the antiproton (-1300 MeV for $\epsilon = 2000$ MeV).

A comparison of the results for the Schrödinger-equivalent potential obtained in the framework of the σ-ω model and the real part of the $\bar{p}$ self-energy resulting from the dispersive approach shows strong differences not only in the absolute values but also in their opposite behavior as a function of the kinetic energy. The fact that the real part of the antiproton self-energy cannot be described consistently within different models urges us to treat it as a free parameter in our transport model. We regard the determination of this parameter in comparison with the experimental data as the central goal of our work.

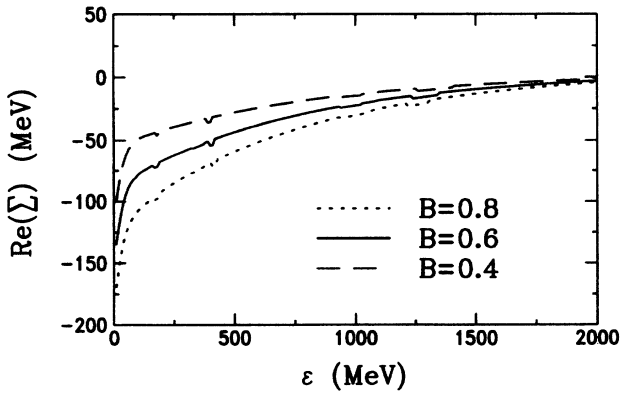

FIG. 2. Real part of the antiproton self-energy as a function of its kinetic energy using different parameters B in the annihilation cross section (6).

III. THE RBUU TRANSPORT APPROACH

In this section we give a brief description of the RBUU model. First we summarize the relevant equations determining the dynamics of baryons and then describe the implementation of antiprotons in our approach.

A. Baryon dynamics

Since the covariant BUU approach has been extensively discussed in the reviews [31,32] and in [33] we only recall the basic equations and the corresponding quasiparticle properties that are relevant for a proper understanding of the results reported in this study. The relativistic BUU (RBUU) equation with momentum-dependent mean fields or self-energies is given by (for details, see Refs. [31–33])

$$\{[\Pi_\mu - \Pi_\nu(\partial^p_\mu U^\nu) + m^*(\partial^p_\mu U_s)]\partial^\mu_x$$

$$+[-\Pi_\nu(\partial^x_\mu U^\nu) + m^*(\partial^x_\mu U_s)]\partial^\mu_p\}f(x,p) = I_{\rm coll}, \quad (10)$$

where $f(x,p)$ is the Lorentz covariant phase-space distribution function, $I_{\rm coll}$ is a collision term [cf., Eq. (19)], and U_s and U_μ are the scalar and the vector self-energies. The effective mass M^* and the kinetic momentum Π_μ are defined in terms of the fields by

$$\Pi_\mu(x,p) = p_\mu - U_\mu(x,p), \quad (11)$$

$$m^*(x,p) = m + U_s(x,p), \quad (12)$$

while the quasiparticle mass-shell constraint is obtained as

$$V(x,p)\,f(x,p) = 0, \quad (13)$$

with the pseudo potential

$$V(x,p) \equiv \frac{1}{2}\{\Pi^2(x,p) - m^{*2}(x,p)\}. \quad (14)$$

The above equation implies that the phase-space distribution function $f(x,p)$ is nonvanishing only on the hypersurface in phase space defined by $V(x,p) = 0$.

In order to implement proper self-energies for the nucleons in line with elastic proton-nucleus scattering we follow Ref. [33] and separate the mean fields into a local part and an explicit momentum-dependent part, i.e.,

$$U_s(x,p) = U_s^H(x) + U_s^{\rm MD}(x,p), \quad (15)$$
$$U_\mu(x,p) = U_\mu^H(x) + U_\mu^{\rm MD}(x,p), \quad (16)$$

where the local mean fields are determined by the usual Hartree equation

$$U_s^H(x) = -g_s\sigma_H(x),$$
$$U_\mu^H(x) = g_v\omega_\mu^H(x), \quad (17)$$

with

$$m_s^2\sigma_H(x) + B_s\sigma_H^2(x) + C_s\sigma_H^3(x) = g_s\rho_s(x),$$
$$m_v^2\omega_\mu^H(x) = g_v j_\mu(x). \quad (18)$$

In the above equations the scalar density $\rho_s(x)$ and the baryon current $j_\mu(x)$ are given in terms of momentum integrals over the phase-space distribution function (cf., [33–35]). The potentials (16) and (15) correct the unphysical strong repulsion in the $p+A$ and $A+A$ potentials at high energies, obtained in the original Walecka model. References. [33,34] give parametrizations which describe both the experimental data and the density-dependence obtained in Brueckner calculations very well.

Now we turn to the discussion of the collision term $I_{\rm coll}$ describing the baryon-baryon collisions (cf. [1,31,36]):

$$I_{\rm coll} = \frac{4}{(2\pi)^5}\int d^3\Pi_1\, d^3\Pi_1'\, d^3\Pi' \frac{m^*\, m_1^*\, m'^*\, m_1'^*}{\Pi^0\,\Pi_1^0\,\Pi'^0\,\Pi_1'^0} W(\Pi^\mu, \Pi_1^\mu \mid \Pi'^\mu, \Pi_1'^\mu)\delta^4(p^\mu + p_1^\mu - p'^\mu - p_1'^\mu)$$
$$\times \{f(x,\Pi')f(x,\Pi_1')[1-f(x,\Pi)][1-f(x,\Pi_1)] - f(x,\Pi)f(x,\Pi_1)[1-f(x,\Pi')][1-f(x,\Pi_1')]\}. \quad (19)$$

This collision integral describes the change in the phase-space distribution function $f(x,\Pi)$ due to the collision of two baryons with effective masses m^*, m_1^* and momenta Π^μ, Π_1^μ, respectively. The two baryons in the final state of the reaction with masses $m'*$ and $m_1'*$ are labeled by their momenta Π' and Π_1'. The δ function guarantees energy and momentum conservation in the individual collision, while $W(\Pi^\mu, \Pi_1^\mu \mid \Pi'^\mu, \Pi_1'^\mu)$ denotes the transition probability for this reaction, which can be expressed in the CMS of the colliding particles by the product of the relative velocity of both colliding particles and the differential cross section for the reaction,

$$W(\Pi^\mu, \Pi_1^\mu \mid \Pi'^\mu, \Pi_1'^\mu) = \left|\frac{\mathbf{\Pi}}{\Pi^0} + \frac{\mathbf{\Pi}}{\Pi_1^0}\right| \frac{d\sigma}{d\Omega}\Big|_{\Pi^\mu+\Pi_1^\mu\to\Pi'^\mu+\Pi_1'^\mu}. \quad (20)$$

For the NN cross section, we use the parametrization given by Cugnon [37] and therefore neglect the possible in-medium corrections. However, the corrections due to Pauli blocking are built in via the factors $1-f$. We explicitly account for the following baryonic channels:

$$N+N \to N+N, N+N \to N+\Delta,$$
$$N+\Delta \to N+N, \Delta+\Delta \to \Delta+\Delta,$$

and propagate the Δ's with the same self-energies as the nucleons. For the parametrizations of the cross sections of reactions including Δ's, see [1].

B. Antiprotons in RBUU

The phase-space distribution function for the antiprotons $f_{\bar p}(x,p_{\bar p})$ is assumed to follow an equation of motion equivalent to Eq. (10), however, with scalar and vector potentials of different strength, i.e.,

$$U_s^{\bar p}(x) = -g_s^{\bar p}\sigma_H(x),$$
$$U_\mu^{\bar p}(x) = g_v^{\bar p}\omega^H(x)_\mu. \quad (21)$$

Thus the effective mass and the effective momentum of antiprotons are given by

$$m_{\bar p}^* = m + U_s^{\bar p}(x) = m - g_s^{\bar p}\sigma_H(x), \quad (22)$$

$$\Pi_\mu^{\bar p} = p_\mu^{\bar p} - U_\mu^{\bar p}(x) = p_\mu^{\bar p} - g_v^{\bar p}\omega^H(x)_\mu. \quad (23)$$

According to the arguments given in Sec. II, the coupling constants $g_s^{\bar p}$ and $g_s^{\bar p}$ are treated as free parameters and will be determined in a comparison of our calculations to

experimental data (cf. Sec. VI). Since at subthreshold energies antiprotons can be produced only in a very limited kinematical range, we can work here with scalar and vector parts of the antiproton self-energies that are not explicitly momentum dependent. We then obtain the following equation of motion for the antiproton phase-space distribution function

$$\left[\frac{\Pi^{\mu}_{\bar{p}}}{\Pi^{0}_{\bar{p}}}\partial^{x}_{\mu}+\left[\Pi^{\nu}_{\bar{p}}F^{\bar{p}}_{\mu\nu}+m^{*}_{\bar{p}}\left(\partial^{x}_{\mu}m^{*}_{\bar{p}}\right)\right]\partial^{\mu}_{\Pi_{\bar{p}}}\right]f_{\bar{p}}(x,\Pi_{\bar{p}}) = I^{\bar{p}}_{\rm coll}(x,\Pi_{\bar{p}}), \quad (24)$$

with

$$F^{\mu\nu}_{\bar{p}}=\partial^{\mu}U^{\bar{p}\,\nu}_{v}-\partial^{\nu}U^{\bar{p}\,\mu}_{v}, \quad (25)$$

and the mass-shell constraint

$$\left(\Pi^{2}_{\bar{p}}-m^{*\,2}_{\bar{p}}\right)\bar{f}\,(x,\Pi_{\bar{p}})=0. \quad (26)$$

The collision term $I^{\bar{p}}_{\rm coll}$ [rhs of Eq. (24)] includes (i) a term $I^{\bar{p}}_{\rm elast}$, describing the elastic antiproton scattering, (ii) a term $I^{\bar{p}}_{\rm prod}$, describing the antiproton production, and (iii) a term $I^{\bar{p}}_{\rm abs}$ responsible for in-medium $\bar{p}$ absorption. $I^{\bar{p}}_{\rm elast}$ describes elastic baryon-antiproton scattering as well as elastic antiproton-antiproton scattering. While this part of the collision integral $I^{\bar{p}}_{\rm coll}$ can be formulated similarly to the collision term describing baryon-baryon scattering (19), the other terms represent extensions to this integral.

1. Collision term for $\bar{p}$ production

The basis for the description of the antiproton production is the reaction

$$B+B\rightarrow\bar{p}+p+N+N\equiv 1+2\rightarrow\bar{p}+3+4+5, \quad (27)$$

for which the corresponding covariant collision integral reads

$$I^{\bar{p}}_{\rm prod}(x,\Pi_{\bar{p}})=\frac{4}{(2\pi)^{11}}\int d^{3}\Pi_{1}\,d^{3}\Pi_{2}\,d^{3}\Pi_{3}\,d^{3}\Pi_{4}\,d^{3}\Pi_{5}\frac{m^{*}_{1}\,m^{*}_{2}\,m^{*}_{3}\,m^{*}_{4}\,m^{*}_{5}\,m^{*}_{\bar{p}}}{\Pi^{0}_{1}\,\Pi^{0}_{2}\,\Pi^{0}_{3}\,\Pi^{0}_{4}\,\Pi^{0}_{5}\,\Pi^{0}_{\bar{p}}}$$
$$\times W(\Pi^{\mu}_{1},\Pi^{\mu}_{2}\mid\Pi^{\mu}_{3},\Pi^{\mu}_{4},\Pi^{\mu}_{5},\Pi^{\mu}_{\bar{p}})\delta^{4}(p^{\mu}_{1}+p^{\mu}_{2}-p^{\mu}_{3}-p^{\mu}_{4}-p^{\mu}_{5}-\Pi^{\mu}_{\bar{p}})$$
$$\times\{f(x,\Pi_{1})f(x,\Pi_{2})[1-f(x,\Pi_{3})][1-f(x,\Pi_{4})][1-f(x,\Pi_{5})]\}. \quad (28)$$

We have omitted the Pauli-blocking factor for the antiproton in the final state because the number of antiprotons created during a heavy-ion collision in the subthreshold energy regime is negligible. For the same reason, we neglect the effects of reaction (27) on the phase-space distribution function of the baryons.

2. Collision term for $\bar{p}$ absorption

In the collision integral $I^{\bar{p}}_{\rm abs}$ we do not treat all possible annihilation reactions separately, but sum up all channels in the inclusive annihilation reaction

$$B+\bar{p}\rightarrow X, \quad (29)$$

where X denotes all possible final states (essentially pions) of the baryon-antiproton annihilation. The corresponding energy and momentum conservation reads

$$p^{\mu}_{B}+p^{\mu}_{\bar{p}}=p^{\mu}_{X}, \quad (30)$$

where p^{μ}_{B} and $p^{\mu}_{\bar{p}}$ denote the 4-momenta of the baryon and the antiproton, respectively, and p^{μ}_{X} stands for the sum of the 4-momenta of all particles in the final state of the annihilation reaction. Reaction (29) then leads to the collision term

$$I^{\bar{p}}_{\rm abs}(x,\Pi_{\bar{p}})=-\frac{4}{(2\pi)^{3}}\int d^{3}\Pi_{1}d^{4}\Pi_{X}\frac{m^{*}_{1}\,m^{*}_{\bar{p}}}{\Pi^{0}_{1}\,\Pi^{0}_{\bar{p}}}$$
$$\times W(\Pi^{\mu}_{1},\Pi^{\mu}_{\bar{p}}\mid\Pi^{\mu}_{X})\delta^{4}(p^{\mu}_{1}+p^{\mu}_{\bar{p}}-p^{\mu}_{X})$$
$$\times f(x,\Pi_{1})f(x,\Pi_{\bar{p}}), \quad (31)$$

with $W(\Pi^{\mu}_{1},\Pi^{\mu}_{\bar{p}}\mid\Pi^{\mu}_{X})$ denoting the transition probability for the reaction (29). Integrating (31) over $d^{4}\Pi_{X}$ implies, in addition to the integration over all final momentum states of a particular reaction, a summation over all possible annihilation channels

$$I^{\bar{p}}_{\rm abs}(x,\Pi_{\bar{p}})=-\frac{4}{(2\pi)^{3}}\int d^{3}\Pi_{1}\frac{m^{*}_{1}\,m^{*}_{\bar{p}}}{\Pi^{0}_{1}\,\Pi^{0}_{\bar{p}}}$$
$$\times W(\Pi^{\mu}_{1},\Pi^{\mu}_{\bar{p}})f(x,\Pi_{1})f(x,\Pi_{\bar{p}}), \quad (32)$$

where $W(\Pi^{\mu}_{1},\Pi^{\mu}_{\bar{p}})$ denotes the probability of an antiproton with effective momentum $\Pi^{\mu}_{\bar{p}}$ annihilating with a baryon with effective momentum Π^{μ}_{1}.

IV. ANTIPROTON PRODUCTION IN RBUU

In this section we describe the numerical treatment of antiproton production in our model and present a systematic analysis of the $\bar{p}$-production mechanism in heavy-ion collisions.

A. Numerical implementation

Since the production probability for antiprotons is very small, the average time evolution of the nucleus-nucleus collision is not affected and it is justified to treat the $\bar{p}$ production perturbatively [2,31]. In this approach the

antiproton invariant differential multiplicity is obtained by summing incoherently over all baryon-baryon collisions and integrating over all residual degrees of freedom. Assuming the antiproton production to take place via reactions of the type

$$B + B \to \bar{p} + p + N + N \equiv 1 + 2 \to \bar{p} + 3 + 4 + 5, \quad (33)$$

(B stands for either nucleon or Δ) the invariant multiplicity as a function of the impact parameter can be written as

$$E_{\bar{p}} \frac{d^3P(b)}{d^3\Pi_{\bar{p}}} = \sum_{BB\text{coll}} \int d^3\Pi_3' d^3\Pi_4' d^3\Pi_5' \frac{1}{\sigma_{BB}(\sqrt{s})} E_{\bar{p}}' \frac{d^{12}\sigma_{BB\to\bar{p}+X}(\sqrt{s})}{d^3\Pi_3' d^3\Pi_4' d^3\Pi_5' d^3\Pi_{\bar{p}}'} [1 - f(x,\Pi_3')][1 - f(x,\Pi_4')][1 - f(x,\Pi_5')], \quad (34)$$

where the quantities $\Pi_i\,(i = 1,...,5)$ denote the in-medium momenta of the participating baryons. $\Pi_{\bar{p}}$ and $E_{\bar{p}}$ stand for the $\bar{p}$-effective momentum and energy, while $s = (\Pi_1^\mu + \Pi_2^\mu)^2$ is the squared invariant energy available in the corresponding baryon-baryon collision. An integration over the impact parameter then yields the Lorentz-invariant differential production cross section

$$E_{\bar{p}} \frac{d^3\sigma_{\bar{p}}}{d^3\Pi_{\bar{p}}} = 2\pi \int db\, b\, E_{\bar{p}} \frac{d^3P(b)}{d^3\Pi_{\bar{p}}}. \quad (35)$$

We assume the elementary antiproton production cross section $\sigma_{BB\to\bar{p}+X}(\sqrt{s})$ in all baryon-baryon channels to be equal to $\sigma_{pp\to\bar{p}+X}(\sqrt{s})$ and employ a parametrization of the free cross section given by [18] (cf. Fig. 3; solid line):

$$\sigma_{BB\to\bar{p}+X} = 0.01(\sqrt{s} - \sqrt{s_0})^{1.846}[\text{mb}], \quad (36)$$

with $\sqrt{s_0} = 4m_N$ and $m_N = 0.9383\,\text{GeV}/c^2$. The dashed and the dotted line in Fig. 3 represent extreme alternative parametrizations that will also be used below.

While in free space the threshold for the elementary production reaction is obviously 4 times the nucleon rest mass in the medium, one additionally has to take into account the self-energies of all participating particles. The conservation of energy and momentum has to be guaranteed, i.e.,

$$p_1^\mu + p_2^\mu = p_3^\mu + p_4^\mu + p_5^\mu + p_{\bar{p}}^\mu, \quad (37)$$

which in terms of effective momenta and self-energies [cf., Eqs. (11) and (23)] yields

$$\Pi_1^\mu + U_v^\mu(|\,\mathbf{p}_1\,|,x) + \Pi_2^\mu + U_v^\mu(|\,\mathbf{p}_2\,|,x) = \Pi_3^\mu + U_v^\mu(|\,\mathbf{p}_3\,|,x) + \Pi_4^\mu + U_v^\mu(|\,\mathbf{p}_4\,|,x) + \Pi_5^\mu + U_v^\mu(|\,\mathbf{p}_5\,|,x) + \Pi_{\bar{p}}^\mu + U_v^{\bar{p}\,\mu}(x). \quad (38)$$

With the abbreviation

$$\Delta^\mu \equiv U_v^\mu(|\,\mathbf{p}_3\,|,x) + U_v^\mu(|\,\mathbf{p}_4\,|,x) + U_v^\mu(|\,\mathbf{p}_5\,|,x) + U_v^{\bar{p}\,\mu}(x) - U_v^\mu(|\,\mathbf{p}_1\,|,x) - U_v^\mu(|\,\mathbf{p}_2\,|,x), \quad (39)$$

we obtain in shorthand form

$$\Pi_1^\mu + \Pi_2^\mu = \Pi_3^\mu + \Pi_4^\mu + \Pi_5^\mu + \Pi_{\bar{p}}^\mu + \Delta^\mu. \quad (40)$$

When evaluating the threshold for the reaction in terms of effective momenta, i.e.,

$$\mathbf{\Pi}_{\bar{p}} + \mathbf{\Pi}_3 + \mathbf{\Pi}_4 + \mathbf{\Pi}_5 = \mathbf{0}, \quad (41)$$

we, in general, encounter a nonvanishing sum of the vector self-energies of all participating particles. This leads to the following expression for the threshold

$$\sqrt{s_0} = \sqrt{(m_{\bar{p}}^* + m_3^* + m_4^* + m_5^* + \Delta^0)^2 - \mathbf{\Delta}^2}. \quad (42)$$

In the σ-ω model, where the $\bar{p}$ self-energies result from the corresponding baryon self-energies by applying charge conjugation, the quantity Δ^μ vanishes and Eq. (42) reduces to an expression equivalent to the free threshold with the rest masses replaced by the effective masses of the participating particles.

In order to derive an expression for the differential $\bar{p}$ multiplicity, we assume, as in Refs. [16–18], that the differential elementary antiproton production cross section is proportional to the phase space available for the final state:

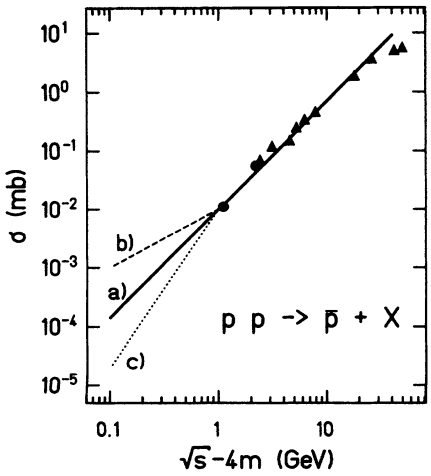

FIG. 3. Inclusive antiproton cross section in a pp collision. The solid line indicates the parametrization (36). The dashed and dotted lines show "extreme" alternative extrapolations to the threshold. The experimental data are taken from [16].

$$E_3E_4E_5E_{\bar{p}}\frac{d^{12}\sigma_{BB\to NNN+\bar{p}}(\sqrt{s})}{d^3\Pi_3 d^3\Pi_4 d^3\Pi_5 d^3\Pi_{\bar{p}}} = \sigma_{BB\to NNN+\bar{p}}(\sqrt{s})\frac{1}{16\,R_4(\sqrt{s})}\delta^4(\Pi_1^\mu+\Pi_2^\mu-\Pi_3^\mu-\Pi_4^\mu-\Pi_5^\mu-\Pi_{\bar{p}}^\mu-\Delta^\mu). \quad (43)$$

Here, the δ function guarantees the energy and momentum conservation and $\sqrt{s}$ is the invariant energy available for the quasiparticles in the initial state. $R_4(\sqrt{s})$ is the 4-body phase-space integral [38]; it has been included to ensure that the differential cross section is normalized to the total cross section.

B. Sensitivity to the elementary cross section

Now we turn first to the analysis of the antiproton production mechanism itself and consequently neglect all in-medium propagation and absorption effects. For the sake of numerical simplicity, we calculate here the $\bar{p}$ production using the baryon self-energies obtained from the nonlinear σ-ω model [39] where the $\bar{p}$ self-energies are determined by charge conjugation from those of the baryons.

Since we are dealing with subthreshold particle production, the antiproton cross section will depend strongly on the behavior of the elementary cross section (36) close to threshold. Since there are no experimental data available for $\sqrt{s}-\sqrt{s_0}\le 1$ GeV (cf. Fig. 3), we have to rely on an extrapolation of the data to threshold. In order to investigate the dependence of our results on the parametrization of the cross section, we display in Fig. 4 the invariant differential production probability for the reaction Si+Si at 2.1 GeV/nucleon for different extreme parametrizations corresponding to the dashed and dotted lines in Fig. 3. This uncertainty of up to one order of magnitude has to be kept in mind when drawing any conclusions from the comparison of our work with the experimental data. For our further analysis we will adopt the parametrization (36).

Due to these uncertainties it is justified to neglect the Pauli-blocking effects in the calculation of antiproton production which turn out to reduce the production probability by about 10 to 20% as shown in Fig. 5 for the special case of a central Au+Au collision at 2.1 GeV/nucleon. The effects of the Pauli-blocking increase with decreasing beam energy and become less important for lighter systems as, e.g., Ne + Ne.

C. Probing the high-density phase with $\bar{p}$

In order to demonstrate the sensitivity of the antiproton production to the equation of state (EOS) for nuclear matter, we display in Fig. 6 the invariant differential $\bar{p}$-production probability for the reactions Au+Au and Si+Si at 2.1 GeV/nucleon calculated for different parametrizations of the EOS. The parameter sets NL1 and NL3 (cf. Ref. [39]) employ the same incompressibility $K = 400$ MeV, but differ in the effective nucleon mass at $\rho=\rho_0$ ($m^*/m = 0.83$ for NL1; $m^*/m = 0.7$ for NL3), while NL1 and NL2 employ the same effective mass, but differ in their incompressibility ($K = 200$ MeV for NL2). For both systems, we observe a production probability which is enhanced by roughly one order of magnitude for NL3 as compared to that from NL1 and NL2. The reason for this behavior is obviously the low-lying threshold which goes along with the small effective nucleon mass when using the parametrization NL3.

While there is hardly any sensitivity to the incompressibility (NL1 versus NL2) in the light system, one can observe an increase of the production probability by a factor of 3 with decreasing incompressibility in the heavy system. The reason for this sensitivity is given in Fig. 7, where we show the differential $\bar{p}$-multiplicity $dN/d\rho$ as a function of the baryon density ρ/ρ_0 at the individual

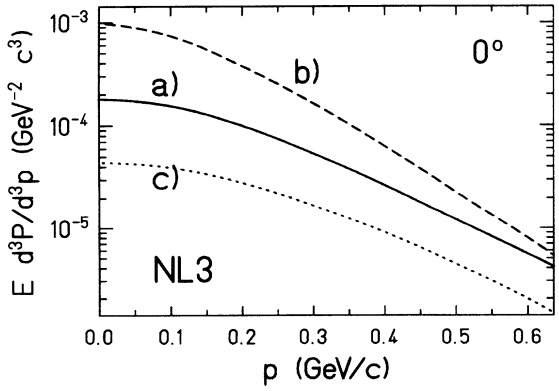

FIG. 4. Invariant differential production probability for Si+Si at 2.1 GeV/nucleon in the CMS ($\Theta = 0°$; $b = 0$; EOS: $K = 200$ MeV, $m^*/m = 0.7$ at $\rho = \rho_0$) using different parametrizations for the elementary production cross section, according to Fig. 3.

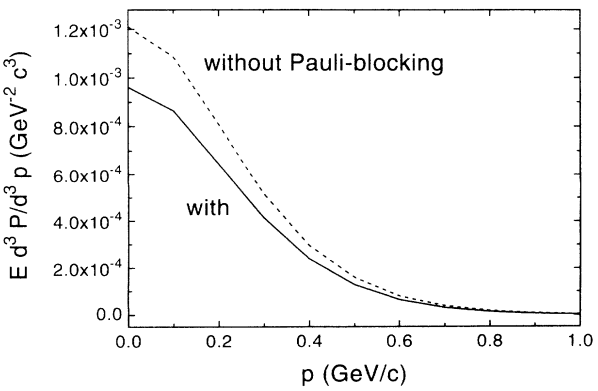

FIG. 5. Effects of Pauli-blocking for Au+Au at 2.1 GeV/nucleon in the CMS ($\Theta = 0°$, $b = 0$); Solid line: Pauli-blocking included; dashed line: no Pauli-blocking.

antiproton production point for Si+Si (dashed line; multiplied by a factor of 50) and Au+Au at 2.1 GeV/nucleon. It is clearly seen that almost all antiprotons are produced at $\rho \geq 3\rho_0$ in the heavy system, while the majority of antiprotons is created between $2\rho_0$ and $3\rho_0$ in the light system. This difference is easily understood in terms of the pileup of density in the heavy system. In the case of Au + Au reactions high densities are obtained for parameter sets that describe a rather soft EOS [40]. Thus compared to NL1 the parameter set NL2 leads to a larger density in the reaction zone, resulting also in a higher antiproton production cross section.

D. Variation with the impact parameter

Since central collisions lead only to minor contributions to the inclusive cross section in heavy-ion collisions, it is of interest to study the $\bar{p}$ multiplicity as a function of the impact parameter b. For this purpose we show in Fig. 8 the calculated differential antiproton multiplicity for Si+Si at 2.1 GeV/nucleon multiplied by $2\pi b$ as a function of b (solid line). This quantity can be approximately fitted by (dotted line)

$$\frac{d\sigma(b)}{db} = 2\pi b\, P(b=0)\; S(b), \tag{44}$$

where $S(b)$ represents the geometrical overlap of two nuclei with mass number A_1 and A_2 as a function of the impact parameter. Assuming $A_1 > A_2$ the overlap function $S(b)$ reads

$$S(b) = \frac{1}{\pi R_2^2}\left\{ R_1^2 \arccos\left[\frac{b^2+R_1^2-R_2^2}{2R_1 b}\right] + R_2^2 \arccos\left[\frac{b^2+R_2^2-R_1^2}{2R_2 b}\right] \right.$$
$$\left. -\frac{1}{4b^2}\left[(b^2+R_1^2-R_2^2)+(b^2+R_2^2-R_1^2)\right]\sqrt{2(R_1^2+R_2^2)\,b^2-b^4-(R_1^2-R_2^2)^2}\right\} \quad \text{for } R_1-R_2 < b < R_1+R_2,$$

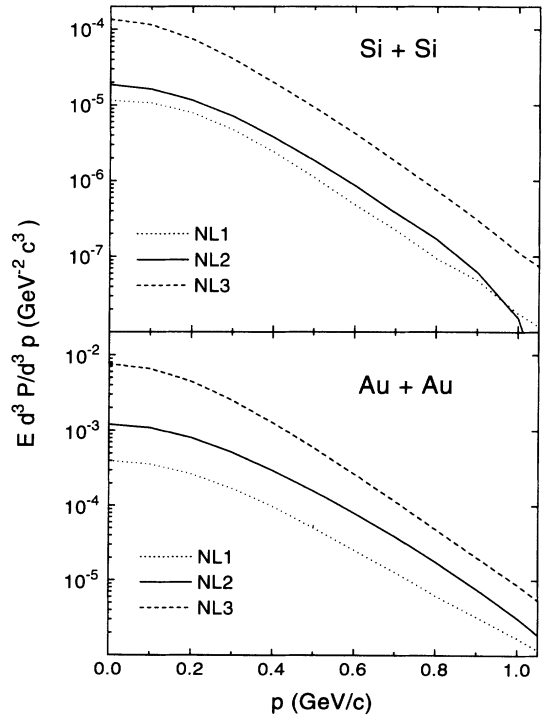

FIG. 6. Differential $\bar{p}$-production probability for Si+Si (top) and Au+Au (bottom) at 2.1 GeV/nucleon in the CMS ($\Theta = 0°$, $b = 0$) using different parametrizations for the EOS; NL1: $K = 400$ MeV, $m^*/m = 0.83$; NL2: $K = 200$ MeV, $m^*/m = 0.83$; NL3: $K = 400$ MeV, $m^*/m = 0.7$ at $\rho = \rho_0$.

and

$$S(b) = 1 \quad \text{for } b \leq R_1 - R_2, \tag{45}$$

with $R_1 = aA_1^{\frac{1}{3}}$, and $R_2 = aA_2^{\frac{1}{3}}$. In case of symmetric systems this reduces to

$$S(b) = \frac{1}{\pi R^2}\left\{ 2R^2 \arccos\frac{b^2}{2Rb} - b\left(R^2-\frac{b^2}{4}\right)^{\frac{1}{2}}\right\}. \tag{46}$$

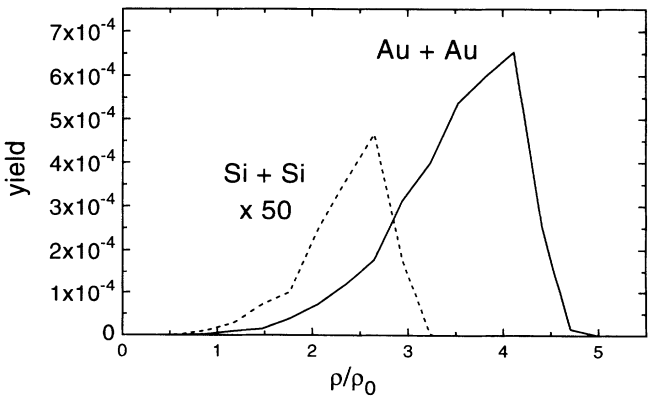

FIG. 7. Production probability as a function of ρ/ρ_0 for Au+Au (solid line) and Si+Si (dashed line; enhanced by a factor of 50) for 2.1 GeV/nucleon; $\Theta_{c.m.} = 0°$, b = 0.

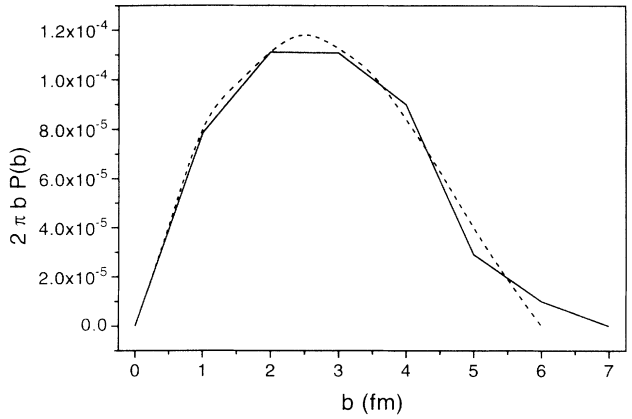

FIG. 8. $\bar{p}$-multiplicity for Si+Si at 2.1 GeV/nucleon as a function of the impact parameter b weighted with $2\pi b$; calculation: solid line; analytic formula: dashed line (cf. text).]

A more systematic analysis with respect to A_1 and A_2 shows that an optimal fit to the impact-parameter dependence is obtained for the radius parameter $a = 1.1$ fm.

E. Baryonic decomposition

It is well known from transport calculations [18,40] that heavy mesons and antiprotons are dominantly produced via multiple baryon-baryon collisions where especially nucleon-resonance channels play an important role. To gain further insight in the mechanism of $\bar{p}$ production, we analyze the relative contribution from various channels in more detail by counting the number of collisions $N_1 + N_2$ that the two baryons have undergone before producing an antiproton in a mutual collision and determine the corresponding production probability as a function of $N_1 + N_2$ for the channels NN, $N\Delta$, and $\Delta\Delta$ separately. The resulting distributions are displayed in Fig. 9 for the reactions Si+Si, Ca+Ca, and Au+Au at 2.0 and 2.5 GeV/nucleon. The full histograms denote the channel $NN \to \bar{p} + X$, the open histograms denote the channel $N\Delta \to \bar{p} + X$, and the hatched histograms the $\Delta\Delta \to \bar{p} + X$, respectively. Table I shows the relative contributions integrated over $N_1 + N_2$. From Table I we can

TABLE I. Relative contributions of the different reaction channels integrated over $N_1 + N_2$.

	2.0 GeV/nucleon			2.5 GeV/nucleon		
	NN	$N\Delta$	$\Delta\Delta$	NN	$N\Delta$	$\Delta\Delta$
Si+Si	5%	45%	50%	10%	52%	38%
Ca+Ca	6%	46%	48%	8%	50%	42%
Au+Au	4%	42%	54%	6%	44%	50%

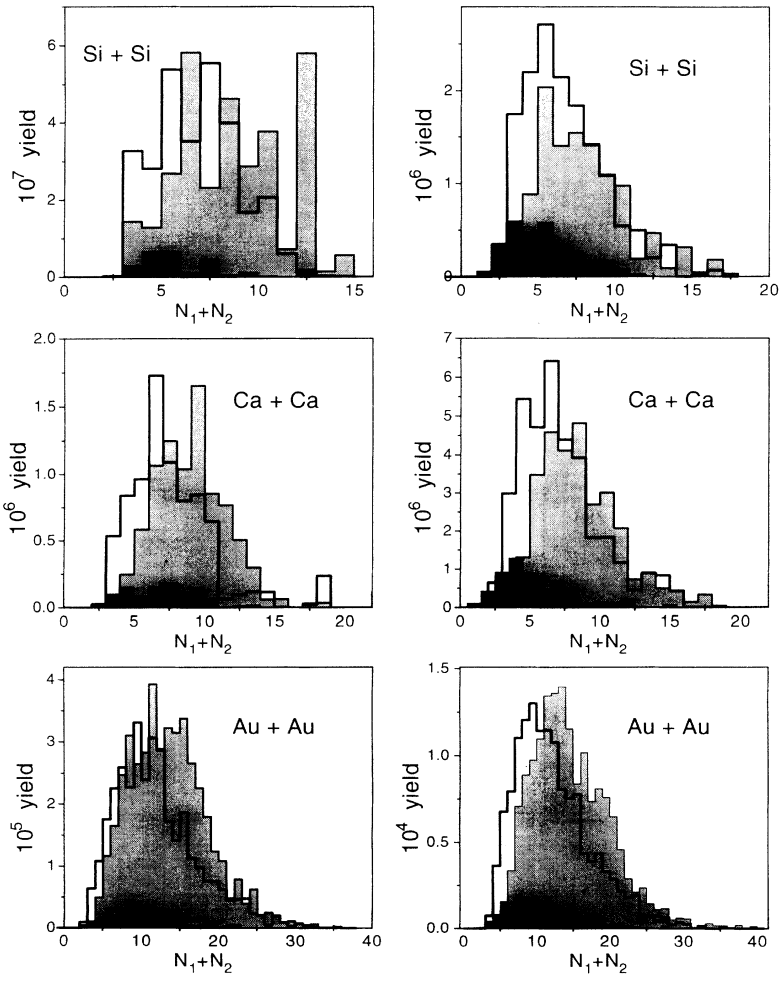

FIG. 9. Contributions to the production from different channels: NN (filled histograms), $N\Delta$ (open histograms), and $\Delta\Delta$ (hatched histograms) for Si+Si, Ca+Ca, and Au+Au at 2.0 GeV/nucleon (left column) and 2.5 GeV/nucleon (right column).

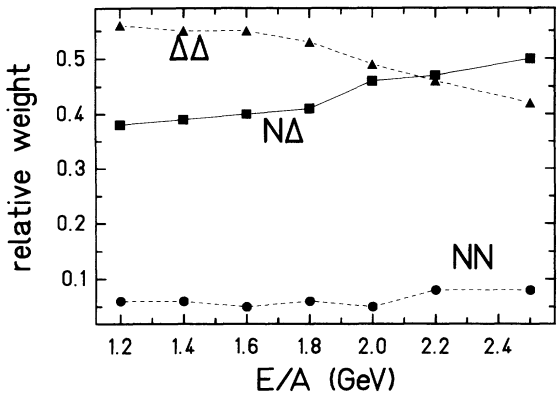

FIG. 10. Relative contributions to the $\bar{p}$ production from different channels as a function of the beam energy for Ca+Ca ($b = 0$); NN (dotted line), $N\Delta$ (solid line), and $\Delta\Delta$ (dashed line).

extract a general trend: The NN channel is obviously of minor importance. In heavier systems the contributions from resonances to the $\bar{p}$ production are generally higher as compared to lighter systems. This correlates with the higher density pileup in heavy systems. The resonances become, furthermore, more important with decreasing beam energy.

In order to study this phenomenon in more detail, we display in Fig. 10 the relative contributions to the $\bar{p}$ yield for Ca+Ca as a function of the beam energy. The contribution from the NN channel is below the 10% level for $E_{\text{beam}} \leq 2.5$ GeV/nucleon. While for higher energies the ΔN channel dominates the production of antiprotons, the $\Delta\Delta$ and the ΔN channel are approximately equally important in the energy regime between 2.4 GeV/nucleon and 2.0 GeV/nucleon. Below 2.0 GeV/nucleon the $\Delta\Delta$ channel is clearly the dominant one.

From the analysis of this section we can conclude that, as far as antiproton production is concerned, the nucleon resonances act as energy reservoirs that can release their energy in baryon-baryon collisions to allow for $\bar{p}$ production. That the resonances are populated in sufficiently large numbers is a consequence of the formation of resonance matter [43] in relativistic heavy-ion collisions.

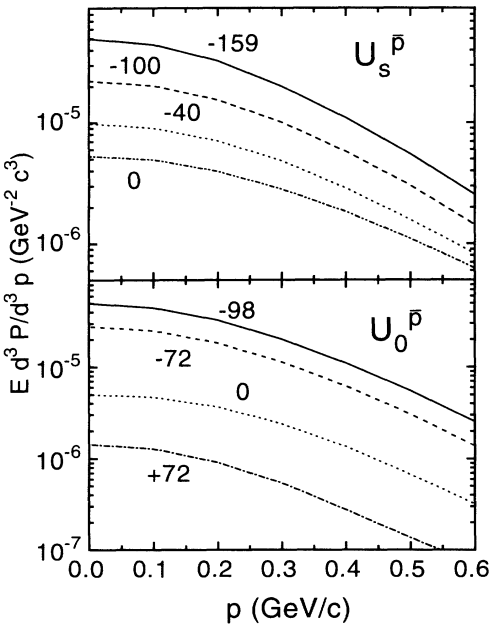

FIG. 11. Differential $\bar{p}$-production probability for a central Ni+Ni collision at 1.85 GeV/nucleon ($\Theta_{\text{CMS}} = 0°$) as a function of the antiproton momentum. Top: fixed $U_0^{\bar{p}} = -98$ MeV at $\rho = \rho_0$ and varying $U_s^{\bar{p}}$ at $\rho = \rho_0$: -159 MeV (solid), -100 MeV (dashed), -40 MeV (dotted), and 0 (dashed-dotted). Bottom: fixed $U_s^{\bar{p}} = -159$ MeV at $\rho = \rho_0$ and varying $U_0^{\bar{p}}$ at $\rho = \rho_0$: -98 MeV (solid), -72 MeV (dashed), 0 (dotted), and $+72$ MeV (dashed-dotted).

F. Sensitivity to in-medium $\bar{p}$ properties

The threshold for the elementary $\bar{p}$-production reaction according to (42) depends on the in-medium properties of the antiprotons. In order to investigate this dependence we calculate the $\bar{p}$-production probability for Ni+Ni at 1.85 GeV/nucleon (central collision) for a variety of different antiproton self-energies: In the calculation shown in the upper part of Fig. 11 the $\bar{p}$-production probability was determined using a fixed vector part of the antiproton self-energy ($U_0^{\bar{p}} = -98$ MeV at $\rho = \rho_0$) while varying the scalar part $U_s^{\bar{p}}$ (see figure caption). The results displayed in the bottom part of Fig. 11 were obtained by varying the vector part while keeping the scalar part $U_s^{\bar{p}}$ fixed at -159 MeV at $\rho = \rho_0$. The same analysis performed for systems other than Ni+Ni lead to quite similar results. Thus we conclude that the antiproton production cross section exhibits an extreme sensitivity to the in-medium $\bar{p}$ properties. This sensitivity will be used below to obtain approximate values for the $\bar{p}$ self-energy in comparison to experimental data.

V. IN-MEDIUM $\bar{P}$ PROPAGATION AND ABSORPTION

The antiprotons produced in individual baryon-baryon collisions can be annihilated while propagating out of the dense nuclear medium. Since we expect the $\bar{p}$ annihilation to dominate the antiproton spectra, a proper treatment of this reaction channel is crucial for a comparison with experimental data. In order to be able to treat the $\bar{p}$ absorption and propagation sufficiently well, we employ a new numerical method which allows us to calculate the propagation as well as the antiproton absorption nonperturbatively. We neglect the elastic scattering of antiprotons with the surrounding baryons; according to Ref. [25] this elastic scattering only causes a flattening of the antiproton momentum spectra. The numerical details of our method are presented in Appendix A. In this section we concentrate on the effects of in-medium absorption and propagation of the antiprotons.

During a heavy-ion collision or a proton-nucleus reac-

tion the antiprotons are created with effective masses $m^*_{\bar{p}}$ and momenta $\Pi^\mu_{\bar{p}}$. These particle properties change according to the surrounding medium as the antiprotons leave the reaction zone. At the end, one observes free antiprotons with canonical momenta $p^\mu_{\bar{p}}$. Since the properties of the antiprotons are determined by their optical potential, one expects significant effects of the $\bar{p}$ propagation on the $\bar{p}$ spectra. We analyze these effects in Figs. 12 and 13. Figure 12 shows the variations in the $\bar{p}$ spectra due to different antiproton self-energies for a central Si+Si collision at 2.1 GeV/nucleon at $\Theta_{\rm lab} = 0°$. The production probability is identical for all cases. The calculations shown in the top part of this figure were performed for $U^{\bar{p}}_s = 0$ and different vector parts (see Fig. 12). The bottom part of this figure shows the result of calculations for $U^{\bar{p}}_\mu = 0$ and varying scalar parts of the antiproton self-energy. Comparing both figures we conclude, as for the $\bar{p}$ production itself, that the effects of the scalar and vector part of the self-energy on the $\bar{p}$ spectra are qualitatively and quantitatively similar. Attractive potentials result in a reduction of the $\bar{p}$ momenta as the antiprotons leave the reaction zone, while repulsive potentials lead to enhanced $\bar{p}$ momenta.

Figure 13 displays the same analysis for p+Cu at 4.0 GeV at $\Theta_{\rm lab} = 0°$. Again, the production was calculated identically for all three cases. Comparing the $\bar{p}$ spectrum obtained for free propagation ($U_{\rm sep} = 0$) with the one obtained using a weakly attractive optical potential ($U_{\rm sep} = -90$ MeV) one observes a slight shift of the spectrum towards lower momenta. This shift is easily explained by the loss of kinetic energy that occurs as the effective mass $m^*_{\bar{p}}$ increases to the value of the rest

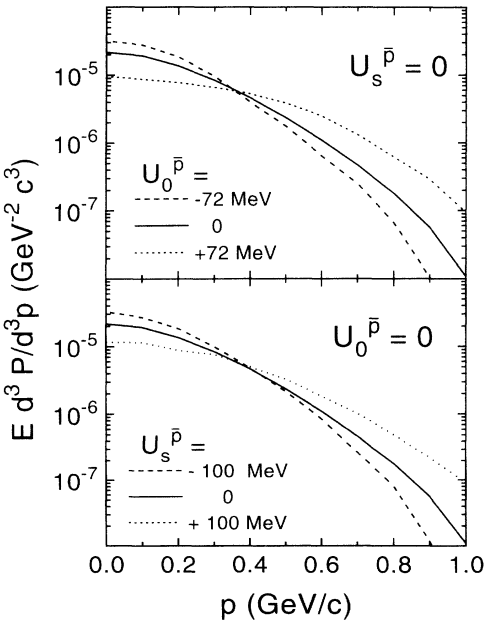

FIG. 12. Effects of the in-medium propagation on the $\bar{p}$ spectrum of Si+Si at 2.1 GeV/nucleon under 0° in the CMS. Top: $U^{\bar{p}}_s = 0$ and $U^{\bar{p}}_0 = -72$ MeV (dashed), 0 (solid), and +72 MeV (dotted) at $\rho = \rho_0$. Bottom: $U^{\bar{p}}_0 = 0$ and $U^{\bar{p}}_s = -100$ MeV (dashed), 0 (solid), and +100 MeV (dotted) at $\rho = \rho_0$.

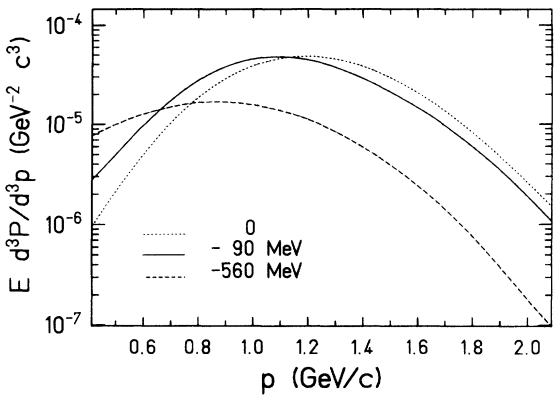

FIG. 13. Effects of the in-medium propagation on the $\bar{p}$ spectrum for the reaction p+Cu at 4.0 GeV, $b = 0$, $\Theta_{lab} = 0°$ for different optical potentials: $U_{\rm sep} = 0$ (dotted), $U_{\rm sep} = -90$ MeV (solid), and $U_{\rm sep} = -560$ MeV (dashed).

mass when the antiprotons leave the reaction zone. Using a strongly attractive optical potential ($U_{\rm sep} = -560$ MeV) one realizes in addition to this shift a reduction of the spectrum due to the propagation effects. Contrary to heavy-ion collisions the target-nuclei in proton-nucleus collisions are not destroyed during those time scales when the antiprotons move into the continuum. This means that the target nuclei build a potential barrier which the antiprotons have to overcome when leaving the nuclei. The low-energy antiprotons cannot overcome this potential wall and get trapped in the nucleus, which leads to the observed reduction in the $\bar{p}$ spectrum.

Figures 12 and 13 clearly show that the antiproton in-medium propagation has an impact on the differential $\bar{p}$ spectra. Therefore it is important to apply the complete mean-field dynamics of the RBUU model when describing the propagation of antiprotons.

Now we turn to the in-medium antiproton absorption ($\bar{p} + B \rightarrow X$). Due to the fact that there is no information available on the in-medium cross section, we have to rely on the free cross section in the parametrization from [13](6). In our transport calculation we replace the free $s - s_0$ with that determined from the in-medium properties of the colliding particles, i.e., $s = (\Pi^0_{\bar{p}} + \Pi^0_B)^2 - (\mathbf{\Pi}_{\bar{p}} + \mathbf{\Pi}_B)^2$ is the squared invariant energy available in the elementary antiproton-baryon collision, while $s_0 = (m^*_{\bar{p}} + m^*_B)^2$ denotes the squared sum of the effective masses of the colliding particles. The dashed line in Fig. 1 represents a cutoff at 100 mb, which is introduced to simulate possible in-medium screening effects. The value of 100 mb for the cutoff is in line with the annihilation radius for proton-antiproton annihilation derived in an optical model calculation [41]. Figure 14 shows the number of antiproton-baryon collisions as a function of the corresponding value of $\sigma_{\rm abs}$ for a central reaction Si+Si at 2.1 GeV/nucleon. Since only a small fraction of all events lies in the region of 100−192 mb, our results do not depend significantly on the cutoff. Similar studies for proton-nucleus collisions show even less sensitivity to this cutoff since the antiprotons move with higher momenta with respect to the target nucleus.

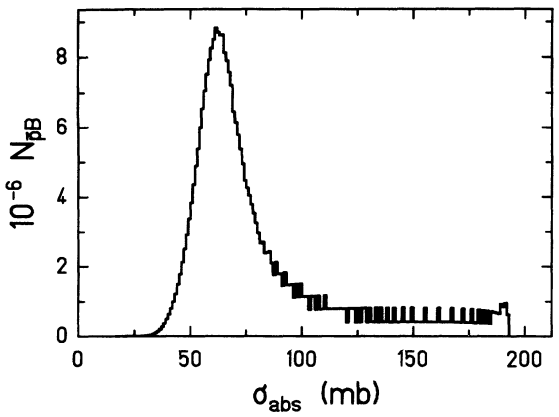

FIG. 14. Number of antiproton-baryon collisions for a central Si+Si reaction at 2.1 GeV/nucleon as a function of the corresponding elementary $\bar{p}$-annihilation cross section.

In order to study the $\bar{p}$-absorption effects on the antiproton spectra from heavy-ion collisions, we have performed calculations using different fixed absorption cross sections in comparison to the dynamically determined cross section (6). Figure 15 shows a full calculation for the system Si+Si at 2.1 GeV/nucleon at $\Theta_{c.m.} = 0°$. The top line denotes the calculated $\bar{p}$ probability without absorption using the baryon self-energies obtained from the nonlinear σ-ω model with $\bar{p}$ self-energies obtained via charge conjugation from the baryon self-energies. The lower lines represent calculations with different constant absorption cross sections, while the solid line results from a calculation using the parametrization (6). This figure clearly reflects the dominant role of the in-medium absorption of antiprotons, which leads to a reduction in $\bar{p}$ probability by approximately two orders of magnitude; these absorption rates agree with those determined by Li *et al.* [25]. Furthermore, the spectral distribution obtained when using the parametrization (6) is—except for small deviations at low antiproton momenta—almost identical to the distribution obtained for a constant cross section of 70 mb. This value corresponds approximately to the mean value of the distribution displayed in Fig. 14.

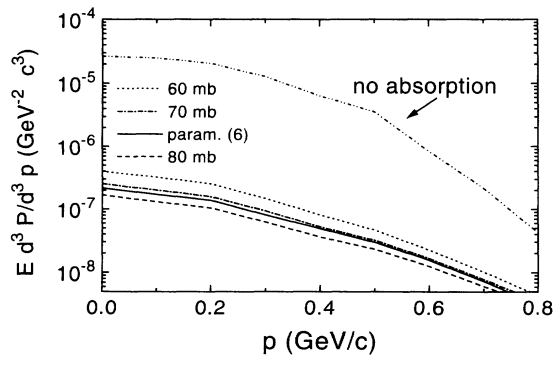

FIG. 15. Antiproton spectra for the reaction Si+Si at 2.1 GeV/nucleon ($b = 0$, $\Theta_{CMS} = 0°$) using different elementary annihilation cross sections: upper line: no absorption; dotted line: $\sigma_{abs} = 60$ mb; dashed-dotted line: $\sigma_{abs} = 70$ mb; solid line: parametrization (6); dashed line: $\sigma_{abs} = 80$ mb.

In this context we note that in proton-nucleus reactions the corresponding mean value of the elementary $\bar{p}$-absorption cross section is approximately 50 mb, which leads to absorption factors of $10 - 30$ depending on the size of the target nucleus and the beam energy. The difference in antiproton absorption between heavy-ion collisions and proton-nucleus reactions is mainly due to the different kinematics in both cases: During a heavy-ion collision most of the antiprotons are created in the CMS of the collision, which implies that the relative velocity of the antiprotons and the surrounding baryonic medium is low. This leads to a small $s - s_0$ for the annihilation reaction and results in high values of the absorption cross section (see Fig. 1). In contrast to this situation the antiprotons produced in proton-nucleus collisions move with momenta of around 1 GeV/c through the baryonic medium, which leads to smaller annihilation rates. Another difference in both types of reactions is that the $\bar{p}$ absorption in proton-nucleus collisions takes place at a maximum density ρ_0, while the antiprotons produced in heavy-ion collisions experience higher densities (cf. Fig. 7), which again leads to an increase in the absorption probability.

Finally, we study the impact-parameter dependence of the antiproton absorption. For this purpose we have to investigate a physical quantity that does not show the impact-parameter dependence of the antiproton production mechanism. The ratio R of the differential $\bar{p}$ probability calculated including absorption and the differential production probability meets this requirement. In Fig. 16 we display R for Ni+Ni at 1.85 GeV/nucleon, Ne+Ni at 2.0 GeV/nucleon, and Si+Si at 2.1 GeV/nucleon as

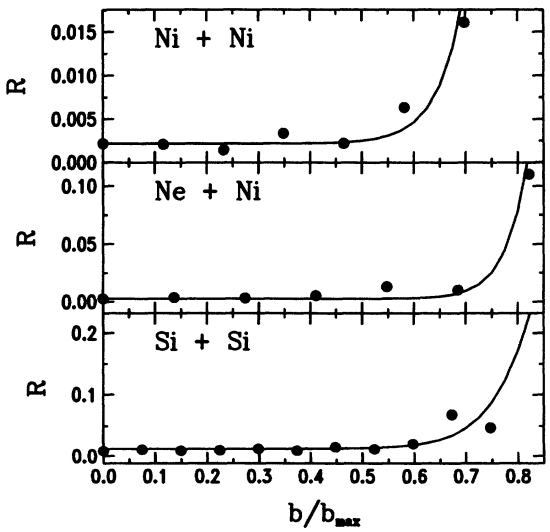

FIG. 16. Quotient R as a function of the impact parameter scaled with b_{max} for the systems Ni+Ni, Ne+Ni, and Si+Si at 1.85 GeV/nucleon, 2.0 GeV/nucleon and 2.1 GeV/nucleon. Dots: RBUU-model; solid lines: fits according to Eq. (47).

TABLE II. Parameters A, B, and C for the fit (47) of R.

	Ni + Ni	Ne + Ni	Si + Si
A	1.0022	1.0025	1.0122
B	0.9	0.9	0.9
C	0.05	0.04	0.06

a function of $b/b_{\max}$ where b denotes the impact parameter and $b_{\max}$ is the sum of the corresponding radii of target and projectile. The ratio R is evaluated for zero antiproton momentum in the CMS of the corresponding heavy-ion collision. The dots represent the values of R calculated in the RBUU model and the solid lines correspond to fits to these numerical data using the function

$$R(b/b_{\max}) = A - \left(1 + e^{\frac{(b/b_{max} - B)}{C}}\right)^{-1}. \quad (47)$$

The parameters A, B, and C are given in Table II. Except for peripheral collisions ($b/b_{\max} > 0.6$), the ratio R is determined by the constant A for all systems. This means that the $\bar{p}$-production spectra for $b/b_{\max} \leq 0.6$ are reduced due to the absorption mechanism by a constant factor determined by the size of the system. The parameters B and C are similar for all systems considered. This leads to the conclusion that the absorption mechanism is similar for all systems and can be understood by means of simple geometrical considerations.

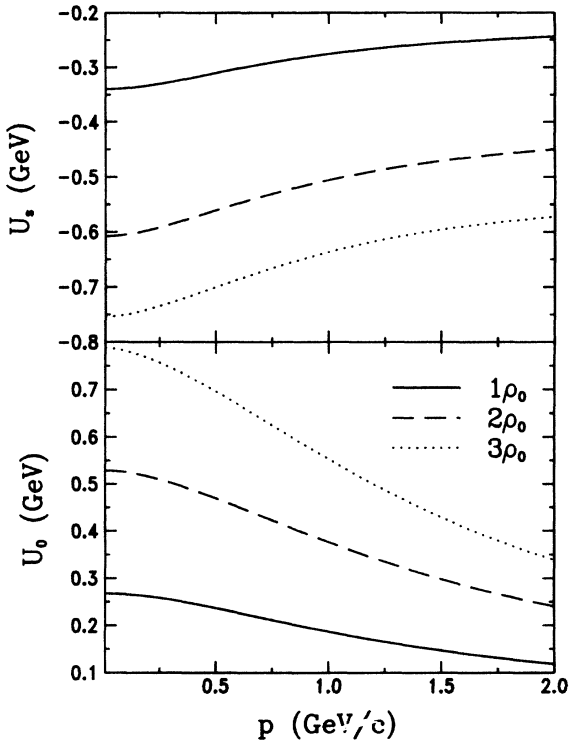

FIG. 17. Scalar and vector self-energies $U_s(p)$ and $U_0(p)$ for nucleons at different densities in units of $\rho_0 \approx 0.17$ fm^{-3}.

VI. COMPARISON WITH EXPERIMENTAL DATA

After the systematic analysis of the in-medium antiproton production and absorption mechanism we now turn to the comparison of our calculations with the most recent data from KEK and GSI. In order to perform this comparison, we describe the $\bar{p}$ self-energies on the basis of the σ-ω-model with free coupling parameters $g_s^{\bar{p}}$ and $g_v^{\bar{p}}$. The comparison with the experimental data will allow us to approximately determine these parameters and then provide first information on the antiproton potential in the dense medium. The quasiparticle properties, i.e., the nucleon self-energies $U_s(x,p), U_\mu(x,p)$ of the baryons participating in the $\bar{p}$-production reaction are taken from Refs. [33–35]. $U_s(x, p)$ and $U_\mu(x, p)$ are fixed to reproduce the saturation properties of nuclear matter, the empirical proton-nucleus optical potential, as well as the density dependence of U_s and U_μ from Dirac-Brueckner theory [36]. For orientation the actual values for $U_s(p)$ and the zero'th component of the vector field $U_0(p)$ are displayed in Fig. 17 for $\rho_0(\approx 0.17$ fm$^{-3}), 2\rho_0$, and $3\rho_0$.

Before we present the results of the calculations using these expressions for the baryon self-energies, we give a brief description of the numerical method used to implement these self-energies into the antiproton production process. Since we deal with explicit momentum dependent self-energies [$U_s(x, p)$, $U_\mu(x, p)$] for the baryons, their effective momenta and masses are given by

$$\Pi_j^\mu = p_j^\mu - U_v^\mu(\mid \mathbf{p}_j \mid, x), \quad (48)$$

$$m_j^* = m + U_s(\mid \mathbf{p}_j \mid, x), \quad j = 1, \ldots, 5, \quad (49)$$

while the corresponding quantities for the antiprotons read

$$\Pi_{\bar{p}}^\mu = p_{\bar{p}}^\mu - U_v^{\bar{p}\,\mu}(x), \quad (50)$$

$$m_{\bar{p}}^* = m + U_s^{\bar{p}}(x). \quad (51)$$

The elementary $\bar{p}$-production events occurring at location $\mathbf{x}$ are evaluated in the corresponding local rest frame (LRF) of the nuclear matter [$j_\mu = (\rho, 0, 0, 0)$]. In this frame the spatial components of the vector self-energies vanish by definition. This implies that the vector components of the effective and the canonical momenta of all particles are the same (48, 50). The spatial components of the quantity Δ^μ defined in Eq. (39) also vanish. Energy and momentum conservation then yields

$$\Pi_1^0 + \Pi_2^0 = \Pi_3^0 + \Pi_4^0 + \Pi_5^0 + \Pi_{\bar{p}}^0 + \Delta^0, \quad (52)$$

$$\mathbf{p}_1 + \mathbf{p}_2 = \mathbf{p}_3 + \mathbf{p}_4 + \mathbf{p}_5 + \mathbf{p}_{\bar{p}}. \quad (53)$$

In order to calculate the $\bar{p}$-production probability we first have to evaluate the threshold $\sqrt{s_0}$ in the LRF. In the CMS of the particles in the final state the threshold is obtained for the kinematical situation with all particles at rest. Thus in the LRF these particles move at threshold with identical velocities. The momenta of the baryons and the antiproton do not necessarily have to be equal because the effective masses of the nucleons and the antiproton can differ from each other. In order to guarantee momentum conservation, we use the following

ansatz for the effective masses of the baryons and the antiprotons

$$|\,\mathbf{p}_j\,| = \frac{m^*(|\,\mathbf{p}_j\,|)}{3m^*(|\,\mathbf{p}_j\,|) + m^*_{\bar{p}}}\,|\,\mathbf{p}_1 + \mathbf{p}_2\,|, \tag{54}$$

$$|\,\mathbf{p}_{\bar{p}}\,| = \frac{m^*_{\bar{p}}}{3m^*(|\,\mathbf{p}_j\,|) + m^*_{\bar{p}}}\,|\,\mathbf{p}_1 + \mathbf{p}_2\,|\,. \tag{55}$$

Since each baryon mass depends itself on the momentum of the corresponding baryon, these equations are iterative equations for the absolute value of the momenta. Using these effective masses the threshold for antiproton production in the LRF reads

$$\sqrt{s_0} = \sqrt{(3\Pi_j^0 + \Pi_{\bar{p}}^0 + \Delta^0)^2 - (3\mathbf{\Pi}_j + \mathbf{\Pi}_{\bar{p}})^2}. \tag{56}$$

$\bar{p}$ production takes place if the invariant energy $\sqrt{s}$ [$s = (\Pi_1^0 + \Pi_2^0)^2 - (\mathbf{\Pi}_1^2 + \mathbf{\Pi}_2^0)^2$] of the baryons in the initial channel lies above the threshold $\sqrt{s_0}$. According to definition (43) the elementary antiproton production cross section is a function of the invariant energy $\sqrt{s'}$ available for the particles in the final state of the production reaction

$$\sqrt{s'} = \sqrt{(\Pi_3^0 + \Pi_4^0 + \Pi_5^0 + \Pi_{\bar{p}}^0)^2 - (\mathbf{p}_3 + \mathbf{p}_4 + \mathbf{p}_5 + \mathbf{p}_{\bar{p}})^2}. \tag{57}$$

Using (52) and (53) this reads

$$\sqrt{s'} = \sqrt{(\Pi_1^0 + \Pi_2^0 - \Delta^0)^2 - (\mathbf{p}_1 + \mathbf{p}_2)^2}. \tag{58}$$

This equation shows that in order to calculate the production probability one has to know the momenta of the particles in the final state of the elementary production reaction when employing momentum-dependent potentials $U_s(x, p)$ and $U_\mu(x, p)$ for the baryons.

Since we are dealing with subthreshold particle production, the main contribution to the production cross section will arise from events with colinear baryon momenta because this kinematical situation minimizes the kinetic energy of the baryons. Based on this argument we assume for the momenta of the baryons in the final state

$$\mathbf{p}_j = \frac{1}{3}(\mathbf{p}_1 + \mathbf{p}_2 - \mathbf{p}_{\bar{p}}). \tag{59}$$

We have applied the above-mentioned formalism to evaluate the antiproton cross section for the reactions p+^{12}C and p+^{63}Cu at bombarding energies of 5, 4, and 3.5 GeV. The corresponding invariant cross sections in comparison with the data of Ref. [11] are shown in Fig. 18 as a function of the momentum of the emitted antiproton in the laboratory frame at $\Theta = 0°$ assuming free antiprotons, i.e., $g_s^{\bar{p}}, g_v^{\bar{p}} = 0$. The calculations slightly underestimate the experimental data, but already approximately reproduce the shape of the momentum spectra as well as the dependence on bombarding energy and mass. The $\bar{p}$ reabsorption amounts to a factor of 12 in the case of ^{12}C and to a factor of 19 for ^{63}Cu, roughly in line with simple geometrical estimates.

When adjusting the constant $g_s^{\bar{p}}$ such that the scalar potential (17) becomes slightly attractive (-50 to -100 MeV at ρ_0) the reproduction of the data improves at all energies significantly, which is exemplified for 4.0 GeV by the dashed line in Fig. 18. In the above comparison we cannot distinguish between scalar and vector antiproton self-energies because both yield similar results for the $\bar{p}$ spectrum if the same Schrödinger-equivalent optical potential is achieved. Furthermore, when using antiproton self-energies in line with the relativistic mean-field theories [30], i.e., changing only the sign of the nucleon vector potential, we overestimate the $\bar{p}$ yield by more than an order of magnitude at all energies for both systems.

We now turn to the nucleus-nucleus case. The calculated antiproton invariant differential cross section for the reaction ^{28}Si+^{28}Si at 2.1 GeV/A and Ni + Ni at 1.85 GeV/nucleon is shown in Fig. 19 in comparison to the experimental data of Ref. [9] and Ref. [12]; the upper lines represent the results of the calculations for free

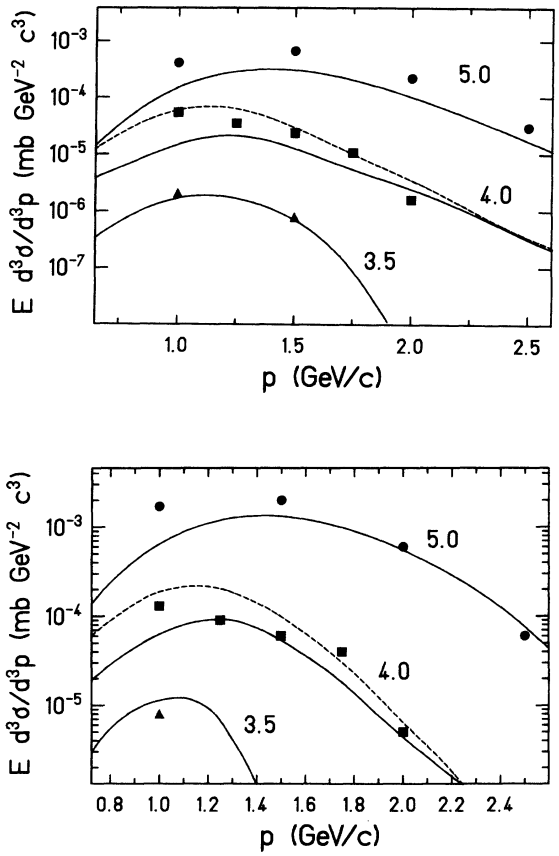

FIG. 18. Invariant cross section for antiproton production in the reactions p+^{12}C (top) and p+^{63}Cu (bottom) at $\Theta = 0°$ as a function of the antiproton momentum p in the laboratory system. The experimental data are taken from Ref. [11] and correspond to bombarding energies of 5.0 GeV, 4.0 GeV, and 3.5 GeV. The full lines represent calculations for free antiprotons. The dashed lines indicate the result for an antiproton self-energy of -100 MeV at 4.0 GeV.

antiprotons without including any reabsorption. When taking care of antiproton annihilation according to Eq. (A2) the yields drop to the lower full lines. In the case of Ni+Ni the data are now underestimated sizeably. However, using attractive scalar (or vector) self-energies at $\rho = \rho_0$ of about -100 to -150 MeV we reproduce the data for Ni+Ni, for Si+Si, however, we miss the data point at $p = 1$ GeV/c.

We thus use a potential of -100 MeV at $\rho = \rho_0$ to predict the differential $\bar{p}$-excitation function in Ni + Ni collisions from 1.4 to 2.5 GeV/nucleon (Fig. 20), a system that will be explored at GSI in the near future [42].

The different value for the attractive antiproton field at $\rho = \rho_0$ in $p+A$ and $A+A$ reactions is due to the fact that in $p+A$ collisions the antiprotons move with momenta of 1–2 GeV/c with respect to the nuclear medium, whereas in $A+A$ collisions the antiprotons have smaller momenta

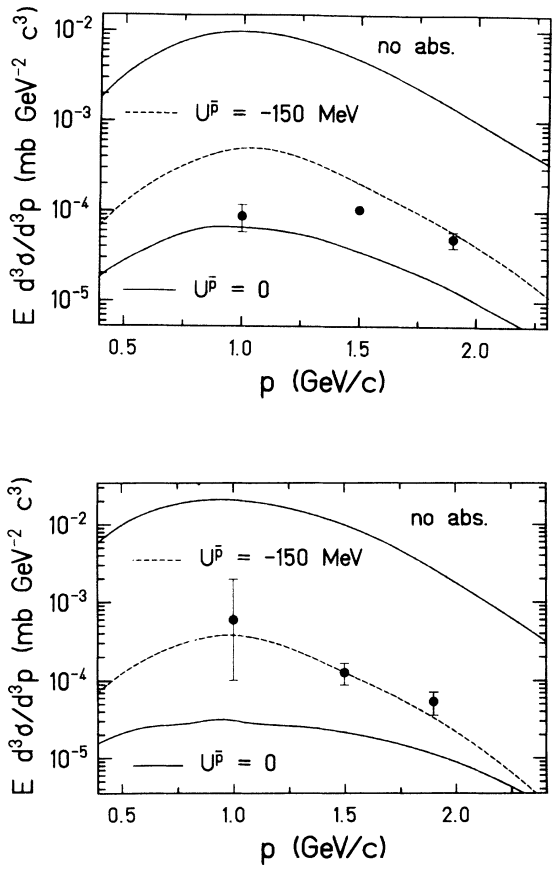

FIG. 19. Invariant cross section for antiproton production in the reaction ^{28}Si+^{28}Si at 2.1 GeV/nucleon (top) and Ni + Ni at 1.85 GeV/nucleon (bottom) for $\Theta = 0°$ as a function of the momentum of the emitted antiproton in the laboratory system. The experimental data have been taken from Refs. [9] and [12], respectively. The upper lines indicate the calculated cross section for free antiprotons without reabsorption whereas the lower solid line is obtained when including $\bar{p}$ annihilation. The dashed line represents the cross section adopting an attractive potential of the antiproton of -150 MeV.

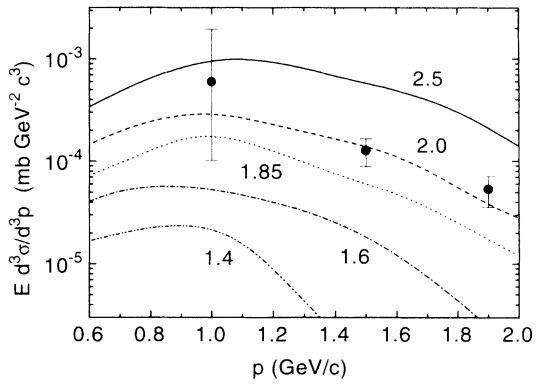

FIG. 20. Invariant cross section for antiproton production in the reaction Ni + Ni at 2.5 GeV/nucleon (solid), 2.0 GeV/nucleon (dashed), 1.85 GeV/nucleon (dotted), 1.6 GeV/nucleon (dotted-dashed), and 1.4 GeV/nucleon (dotted-dotted-dashed). All calculations were done using an attractive $\bar{p}$ potential of -100 MeV at $\rho = \rho_0$. The experimental data are taken from [12].

in the nucleus-nucleus center-of-mass frame. In view of uncertainties of our present studies with respect to the elementary production cross sections close to the thresholds, we provide areas for the antiproton Schrödinger-equivalent potential at $\rho = \rho_0$ in Fig. 21, as extracted from the comparison with the experimental data for $p+A$ and $A + A$ reactions. These areas are far from the values expected by charge conjugation from the familiar σ-ω model [30] (dashed line) and thus exclude relativistic mean-field models with the same parameter sets for nucleons and antinucleons. However, our extracted values are well in line with a Schrödinger-equivalent potential (solid line in Fig. 21) as calculated from the dispersion relation [see Eqs. (1) – (5)]. Crucial for this result is the correct momentum dependence for the $p + A$ potential in the entrance channel. If we use the original

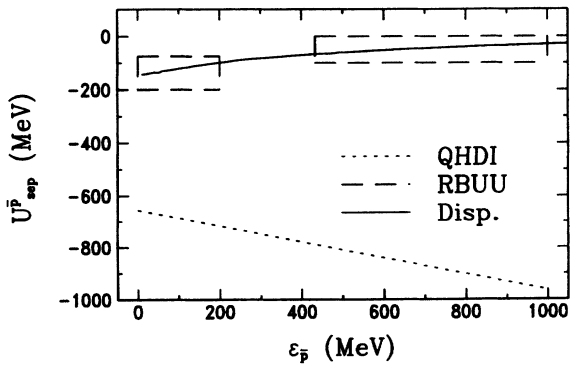

FIG. 21. Comparison of our extracted values for the Schrödinger-equivalent antiproton potential from $p + A$ and $A + A$ reactions with the prediction from the σ-ω model (dashed line) and the dispersive potential according to Eqs. (1)–(5) (solid line).

Walecka model without the momentum-dependent coupling strength we are forced to compensate for the strong repulsion with much deeper antiproton potentials.

The primordial antiproton production rates and the reduction due to absorption obtained here agree well with those obtained by Li *et al.* [25]. These authors also get agreement with the data for Si+Si, however, by using the very deep $\bar{p}$ potential obtained by charge conjugation from the Walecka model and the corresponding strong repulsion in the entrance channel; using the same model we also reproduce the data as well as their calculations within a factor of two. However, the entrance channel potential is much too repulsive, as mentioned in Sec. III B1, so that an unphysically deep antiproton potential is needed to compensate for this repulsion. This fact shows that the conclusion of Ref. [25]—that the agreement of their calculation with the data supports the assumption of a very deep G-parity transformed nucleon potential for the antiprotons—is not justified.

VII. SUMMARY

In this work we have evaluated the differential cross section for $\bar{p}$ production for proton-nucleus and nucleus-nucleus reactions in the subthreshold regime by considering on-shell baryon-baryon production channels involving nucleons and Δ's with their in-medium quasiparticle properties and by treating $\bar{p}$ propagation and annihilation nonperturbatively. The quasiparticle properties of the nucleons are fixed in our approach by the nuclear saturation properties, the proton-nucleus empirical potential, as well as Dirac-Brueckner calculations at higher density. By varying especially the antiproton self-energy, we have shown that the differential $\bar{p}$ spectra are highly sensitive to the antiproton quasiparticle properties. Though we still have to rely on proper extrapolations to the threshold of the elementary process $p + p \rightarrow \bar{p} + X$, the latter sensitivity can be used to obtain approximate values for the $\bar{p}$ Schrödinger-equivalent potential from a systematic comparison to the available experimental data.

In this respect we have performed a systematic study of p-nucleus and nucleus-nucleus collisions in a broad kinematical regime and compared our numerical results to the data from KEK [11] and GSI [12]. We find a consistent description of all data employing a rather weak attractive potential for the antiprotons, which is well in line with a dispersive potential extracted from the dominant imaginary part of the antiproton self-energy due to annihilation. Essential for this result is the use of the correct momentum dependence of the nucleon-nucleus potential in the entrance channel. Although the validity of the simple dispersive model used here may be questionable at higher densities and the extrapolation of the elementary $\bar{p}$-production cross section down to threshold introduces an uncertainty, the consistency of the $\bar{p}$ potentials obtained from a fit to the data with those calculated in the dispersive model indicates that the basic antiproton production mechanism in $p + A$ and $A + A$ reactions is understood.

It has become clear that the baryonic production channels at subthreshold energies involve dominantly one or two nucleon resonances and that the production proceeds at the highest densities that can be reached in a nucleus-nucleus reaction. Only at these high densities the relative population of nucleon resonances ($\approx 30\%$ as shown in [43]) as well as the nucleon-resonance collision rate are high enough to allow for $\bar{p}$ production. Otherwise the resonances decay to a nucleon and a pion before colliding with another baryon such that the energy stored in the resonance gets lost for the production.

We note in closing that the antiproton production studies at the AGS [44–46] around 15 GeV/nucleon, although far above the free production threshold, might yield further information on the dynamics and self-energies of antiprotons at even higher densities.

ACKNOWLEDGMENTS

The authors acknowledge valuable discussions with A. Gillitzer, P. Kienle, W. König, and A. Schröter as well as their information on experimental results prior to publication. They are also very grateful to C. M. Ko for detailed discussions both on the physics and on the computational aspects of these calculations. This work was supported by BMFT, GSI Darmstadt, KFA Jülich, and JSPS.

APPENDIX A: THE WEIGHTED TEST PARTICLE METHOD

In the following we present the weighted test particle method used to implement the antiproton production, absorption, and propagation in the RBUU model. It is especially suited for the simulation of processes with low production probabilities and/or high in-medium absorption cross sections for which conventional test particle methods fail because of low statistics.

Assuming that during a calculation N elementary baryon-baryon collisions with sufficient energy for antiproton production occur, we define for each collision i ($i \in \{1, \ldots, N\}$) a three-dimensional momentum grid in the reference frame (CMS of the heavy-ion collision or lab system). In order to calculate the production probability for each collision i, we transform this grid into the system that fulfills Eq. (41) or into the LRF [see Eqn. (48) to (59)]. After calculating the invariant differential $\bar{p}$-production probability $w^{(i)}_{klm}$ for each grid point $\mathbf{p} = (k\Delta p_x, l\Delta p_y, m\Delta p_z)$ the momentum grid is transformed back into the reference frame. To obtain the total invariant differential production probability without absorption for a heavy-ion collision or a proton-nucleus reaction, one has to sum up the contributions from all the N elementary production reactions

$$W_{klm} = \sum_{i=1}^{N} w^{(i)}_{klm}. \tag{A1}$$

In order to calculate the antiproton probability including propagation through the dense medium and absorption, we start out with the momentum grid described above. For all N baryon-baryon collisions contributing to the antiproton production we place a test particle representing an antiproton on every point of the momentum grid. This yields additional j ($j = k \cdot l \cdot m$) test particles for each of the N baryon-baryon collision events. The effective masses and momenta of these test particles are determined according to both the location on the momentum grid and the spatial coordinate where the baryon-baryon collision takes place. In addition, we attach variable weights to the test particles. The weight $w_h'^{(i)}$ of the h th test particles "created" in the ith collision denotes the invariant differential production probability $w_{klm}^{(i)}$ at the corresponding grid point. The result of this procedure is an ensemble of test particles representing the produced antiprotons that contain information about the differential $\bar{p}$ distribution for each relevant baryon-baryon collision. The entire test particle distribution together with the corresponding weights represents the phase-space distribution of the antiprotons produced in a heavy-ion collision or a proton-nucleus reaction.

We now describe how we treat this ensemble of test particles in order to calculate the antiproton propagation and absorption: Each test particle is propagated by means of the equation of motion for the antiparticle phase-space distribution function (24). At the end of each time step the absorption rate for the test particles is calculated according to their weights. In order to perform this task we convert the collision integral (32) into a differential equation for the test particle weights

$$\left.\frac{dw_h'^{(i)}}{dt}\right|_{x,\Pi_{\bar{p}}} = -\frac{4}{(2\pi)^3}\int\int \frac{d^3\Pi_B}{\Pi_B^0} d^4\Pi_X m_B^* W(\bar{p}+B\to X)\delta^4(\Pi_{\bar{p}}^\mu + \Pi_B^\mu - \Pi_X^\mu) f(x^\mu, \Pi_B^\mu) w_h'^{(i)}\Big|_{x,\Pi_{\bar{p}}}, \tag{A2}$$

where x^μ is the space-time coordinate where the annihilation takes place. $\Pi_{\bar{p}}$, Π_B, $m_{\bar{p}}^*$, and m_B^* denote the effective momenta and masses of the antiprotons and the baryons, respectively. This differential equation leads to the following changes in the test particle weights in time steps Δt,

$$\begin{aligned} w'(t_{j+1})_h^{(i)} &= w'(t_j+\Delta t)_h^{(i)} \\ &= w'(t_j)_h^{(i)} \exp\left[-\int_{t_j}^{t_{j+1}}\int \frac{d^3\Pi_B}{\Pi_B^0} m_B^* W(\bar{p}+B\to X) f(x^\mu,\Pi_B^\mu) dt\right]. \end{aligned} \tag{A3}$$

Solving the integral in the exponent of (A3) by means of the local density approximation (LDA) [47] leads to

$$w'(t_{j+1})_h^{(i)} = w'(t_j)_h^{(i)} \exp\left[-\frac{1}{\Delta V N_t}\sum_{j\in V_i}\left|\frac{\mathbf{\Pi}_{\bar{p}}}{\Pi_{\bar{p}}^0} - \frac{\mathbf{\Pi}_{B_j}}{\Pi_{B_j}^0}\right| \sigma(\bar{p}+B_j\to X)\Delta t\right], \tag{A4}$$

with N_t being the number of test particles per nucleon used to model the baryon phase-space distribution, and ΔV being the normalization volume used in the RBUU model to evaluate densities and currents. Equation (A4) allows for a nonperturbative evaluation of high absorption rates without a reduction of the number of test particles.

At the end of the simulation we project the weight of each antiproton test particle obtained in the final time step t_f of our calculation on the three-dimensional momentum grid (see above)

$$\tilde{w}'^{(i)}_h(t_f, p_x, p_y, p_z) \to \tilde{w}'^{(i)}_{klm}, \tag{A5}$$

and sum up all contributions in order to obtain the invariant differential antiproton probability for the corresponding heavy-ion collision or proton-nucleus reaction.

[1] G. F. Bertsch and S. das Gupta, Phys. Rep. **160**, 189 (1988).
[2] W. Cassing, V. Metag, U. Mosel, and K. Niita, Phys. Rep. **188**, 363 (1990).
[3] U. Mosel, Annu. Rev. Nucl. Part. Sci. **41**, 29 (1991).
[4] J. Aichelin, Phys. Rep. **202**, 235 (1991).
[5] O. Chamberlain, W. W. Chupp, G. Goldhaber, E. Segre, and C. Wiegand, Il Nuovo Cimento **3**, 447 (1956).
[6] T. Elioff, L. Agnew, O. Chamberlain, H. M. Steiner, C. Wiegand, and T. Ypsilantis, Phys. Rev. **128**, 869 (1962).
[7] D. E. Dorfan, J. Eades, L. M. Ledermann, W. Lee, and C. C. Ting, Phys. Rev. Lett. **14**, 995 (1965).
[8] A. A. Baldin *et al.*, JETP Lett. **48**, 137 (1988).
[9] J. B. Carroll *et al.*, Phys. Rev. Lett. **62** 1829 (1989).
[10] A. Shor *et al.*, Phys. Rev. Lett. **63**, 2192 (1989).
[11] J. Chiba *et al.*, Nucl. Phys. **A553**, 771c (1993).
[12] A. Schröter, E. Berdermann, H. Geissel, A. Gillitzer, J. Homolka, P. Kienle, W. König, B. Povh, F. Schumacher, and H. Ströher, Nucl. Phys. **A553**, 775c (1993).
[13] P. Koch and C. B. Dover, Phys. Rev. C **40**, 145 (1989).
[14] C. M. Ko and X. Ge, Phys. Lett. B **205**, 195 (1988).
[15] C. M. Ko and L. H. Xia, Phys. Rev. C **40**, R1118 (1989).

[16] P. Danielewicz, Phys. Rev. C **42**, 1564 (1990).
[17] A. Shor, V. Perez-Mendez, and K. Ganezer, Nucl. Phys. **A514**, 717 (1990).
[18] G. Batko, W. Cassing, U. Mosel, K. Niita, and Gy. Wolf, Phys. Lett. B **256**, 331 (1991).
[19] S. W. Huang, G. Q. Li, T. Maruyama, and A. Faessler, Nucl. Phys. **A547**, 653 (1992).
[20] J. Schaffner, I. N. Mishustin, L. M. Satarov, H. Stöcker, and W. Greiner, Z. Phys. A **341**, 47 (1991).
[21] K. Soutome, T. Maruyama, and K. Saito, Nucl. Phys. **A507**, 731 (1990).
[22] A. Lang, B. Blättel, V. Koch, K. Weber, W. Cassing, and U. Mosel, Phys. Lett. B **245**, 147 (1990).
[23] W. Cassing, A. Lang, S. Teis, and K. Weber, Nucl. Phys. **A545**, 123c (1992).
[24] S. Teis, W. Cassing, T. Maruyama, and U. Mosel, Phys. Lett. B **319**, 47 (1993).
[25] G. Q. Li, C. M. Ko, X. S. Fang, and Y. M. Zheng, submitted to Phys. Rev. C.
[26] T. Walcher, Annu. Rev. Nucl. Part. Sci. **38**, 67 (1989).
[27] C. Amsler, Annu. Rev. Nucl. Part. Sci. **41**, 219 (1991).
[28] V. Flaminio *et al.*, CERN-HERA Report 84-01, 1984.
[29] S. Janouin, M. C. Lemaire, D. Garreta, P. Birien, G. Bruge, D. M. Drake, D. Legrand, B. Mayer, J. Pain, and J. C. Peng, Nucl. Phys. **A451**, 541 (1986).
[30] B. D. Serot and J. D. Walecka, Adv. Nucl. Phys. **16**, 1 (1986).
[31] W. Cassing and U. Mosel, Prog. Part. Phys. **25**, 235 (1990).
[32] B. Blättel, V. Koch, and U. Mosel, Rep. Prog. Phys. **56**, 1 (1993).
[33] K. Weber, B. Blättel, W. Cassing, H. C. Dönges, V. Koch, A. Lang, and U. Mosel, Nucl. Phys. **A539**, 713 (1992).
[34] K. Weber, B. Blättel, W. Cassing, H. C. Dönges, A. Lang, T. Maruyama, and U. Mosel, Nucl. Phys. **A552**, 571 (1993).
[35] T. Maruyama, B. Blättel, W. Cassing, A. Lang, U. Mosel, and K. Weber, Phys. Lett. B **297**, 228 (1992).
[36] W. Botermans and R. Malfliet, Phys. Rep. **198**, 115 (1990).
[37] J. Cugnon, T. Mizutani, and J. Vandermeulen, Nucl. Phys. **A352**, 505 (1981).
[38] E. Byckling and K. Kajantie, *Particle Kinematics* (Wiley, London, 1973).
[39] A. Lang, B. Blättel, W. Cassing, V. Koch, U. Mosel, and K. Weber, Z. Phys. A **341** (1991).
[40] A. Lang, W. Cassing, U. Mosel, and K. Weber, Nucl. Phys. **A541**, 507 (1992).
[41] W. Weise, Nucl. Phys. **A558**, 219c (1993).
[42] P. Kienle, private communication.
[43] W. Ehehalt, W. Cassing, A. Engel, U. Mosel, and Gy. Wolf, Phys. Rev. C **47**, R2467 (1993).
[44] V. Koch and G. E. Brown, Phys. Lett. B **265**, 29 (1991).
[45] A. Jahns, H. Stöcker, and W. Greiner, Phys. Rev. Lett. **68**, 2895 (1992).
[46] S. H. Kahana, Y. Pang, T. Schlagel, and C. B. Dover, Phys. Rev. C **47**, 1356 (1993).
[47] A. Lang, H. Babovsky, W. Cassing, U. Mosel, H.-G. Reusch, and K. Weber, J. Comput. Phys. **106**, 391 (1993).

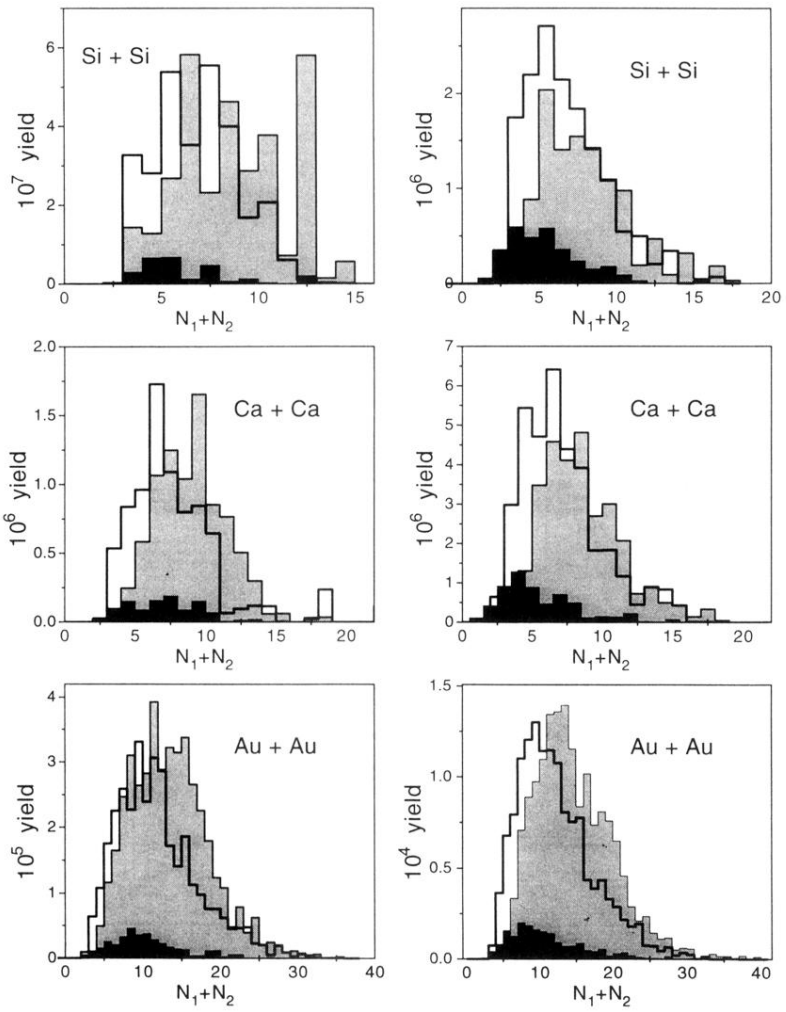

FIG. 9. Contributions to the production from different channels: NN (filled histograms), $N\Delta$ (open histograms), and $\Delta\Delta$ (hatched histograms) for Si+Si, Ca+Ca, and Au+Au at 2.0 GeV/nucleon (left column) and 2.5 GeV/nucleon (right column).